Journal of Applied Mechanics

Brief Notes

A Brief Note is a short paper that presents a specific solution of technical interest in mechanics but which does not necessarily contain new general methods or results. A Brief Note should not exceed 1500 words *or equivalent* (a typical one-column figure or table is equivalent to 250 words; a one line equation to 30 words). Brief Notes will be subject to the usual review procedures prior to publication. After approval such Notes will be published as soon as possible. The Notes should be submitted to the Technical Editor of the JOURNAL OF APPLIED MECHANICS. Discussions on the Brief Notes should be addressed to the Editorial Department, ASME, United Engineering Center, Three Park Avenue, New York, NY 10016-5990, or to the Technical Editor of the JOURNAL OF APPLIED MECHANICS. Discussions on Brief Notes appearing in this issue will be accepted until two months after publication. Readers who need more time to prepare a Discussion should request an extension of the deadline from the Editorial Department.

Asymmetric Four-Point Crack Specimen

M. Y. He
Materials Engineering Department, University of California, Santa Barbara, CA 93106

J. W. Hutchinson
Fellow ASME, Division of Engineering and Applied Sciences, Harvard University, Cambridge, MA 02138

Accurate results for the stress intensity factors for the asymmetric four-point bend specimen with an edge crack are presented. A basic solution for an infinitely long specimen loaded by a constant shear force and a linear moment distribution provides the reference on which the finite geometry solution is based.
[S0021-8936(00)03601-1]

This note was prompted by a comparison ([1]) of existing numerical solutions ([2–4]) for the crack specimen known as the asymmetric four-point specimen shown in Fig. 1. Discrepancies among the solutions are as large as 25 percent within the parameter range of interest. Moreover, in some instances the full set of nondimensional parameters specifying the geometry (there are four) have not been reported. The specimen has distinct advantages for mixed mode testing, including the determination of mixed mode fatigue crack thresholds. Here a new fundamental reference solution is given for a infinitely long cracked specimen subject to a constant shear force and associated bending moment distribution. The small corrections needed to apply this solution to the finite four-point loading geometry are included.

By static equilibrium (the configuration in Fig. 1 is statically determinant), the shear force, Q, between the inner loading points and the bending moment, M, at the crack are related to the force, P, by (all three quantities are defined *per unit thickness*):

$$Q=P(b_2-b_1)/(b_2+b_1) \quad \text{and} \quad M=cQ. \tag{1}$$

Consider first the reference problem of an infinite specimen with crack of length a subject to a constant shear force Q and associated linearly varying bending moment M. In the absence of the crack, the exact solution for the cross section has a parabolic distribution of shear stress proportional to Q and a linear variation of normal stress proportional to M ([5]). By superposition of these two contributions, the solution for the intensity factors in the presence of the crack can be written exactly in the form

$$K_{\mathrm{I}}^R=\frac{6cQ}{W^2}\sqrt{\pi a}F_{\mathrm{I}}(a/W) \tag{2a}$$

$$K_{\mathrm{II}}^R=\frac{Q}{W^{1/2}}\frac{(a/W)^{3/2}}{(1-a/W)^{1/2}}F_{\mathrm{II}}(a/W) \tag{2b}$$

where, anticipating the application, we have taken $M=cQ$ at the crack. The solution (2a) is the same as that for a pure moment. It has been obtained numerically to considerable accuracy. Tada et al. [6] give

$$F_{\mathrm{I}}\left(\frac{a}{W}\right)=\sqrt{\frac{2W}{\pi a}\tan\frac{\pi a}{2W}}\;\frac{0.923+0.199\left(1-\sin\dfrac{\pi a}{2W}\right)^4}{\cos\dfrac{\pi a}{2W}}$$

$$\text{for } 0\leqslant\frac{a}{W}\leqslant 1 \tag{3a}$$

while Murakami [7] gives

$$F_{\mathrm{I}}\left(\frac{a}{W}\right)=1.122-1.121\left(\frac{a}{W}\right)+3.740\left(\frac{a}{W}\right)^2+3.873\left(\frac{a}{W}\right)^3$$
$$-19.05\left(\frac{a}{W}\right)^4+22.55\left(\frac{a}{W}\right)^5 \quad \text{for } \frac{a}{W}\leqslant 0.7. \tag{3b}$$

The second solution (2b) is not in the literature.

Finite element analyses of the reference problem have been carried out to obtain both F_{I} (as a check) and F_{II}. Our results for F_{I} agree with (3b) to four significant figures over the entire range

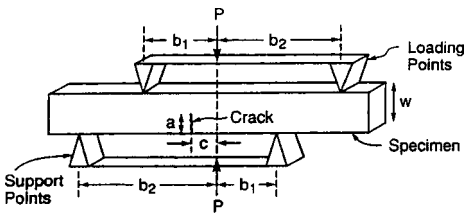

Fig. 1 Geometry of the asymmetric bending and shear specimen

Contributed by the Applied Mechanics Division of THE AMERICAN SOCIETY OF MECHANICAL ENGINEERS for publication in the ASME JOURNAL OF APPLIED MECHANICS. Manuscript received and accepted by the ASME Applied Mechanics Division, Feb. 22, 1999. Associate Technical Editor: A. Needleman.

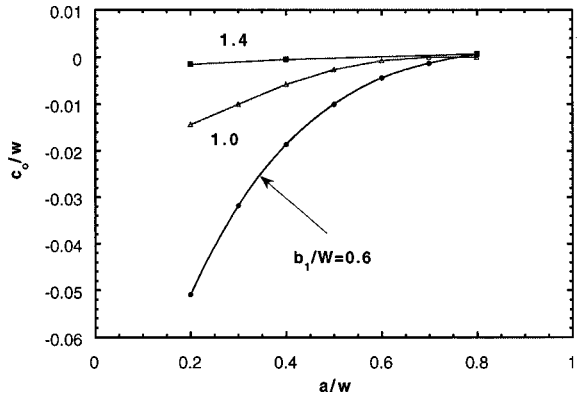

Fig. 2 Location of the crack for pure mode II at its tip ($\alpha=1$)

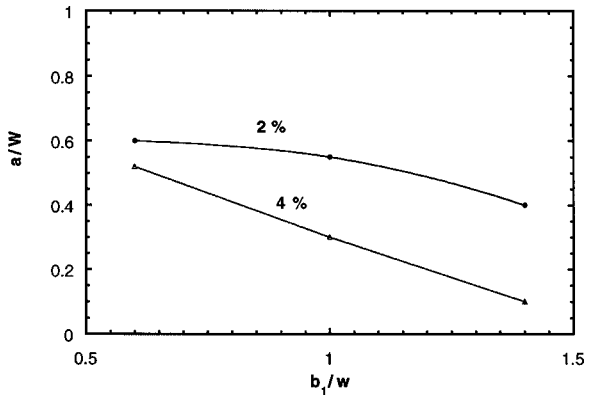

Fig. 4 Error boundaries for mode II stress intensity factor of two percent and four percent for ($\alpha=1$) for the reference solution (2). Combinations ($a/W, b_1/W$) lying above a boundary have smaller error.

of a/W indicated. Equation (3*a*) appears to be less accurate over this same range (with error less than two percent), but it can be used for $a/W>0.7$. The same finite element meshes were used to compute F_{II}. The following polynomial representation was obtained by fitting the numerical results:

$$F_{\mathrm{II}}\left(\frac{a}{W}\right)=7.264-9.37\left(\frac{a}{W}\right)+2.74\left(\frac{a}{W}\right)^2+1.87\left(\frac{a}{W}\right)^3 -1.04\left(\frac{a}{W}\right)^4 \quad \text{for} \quad 0\leqslant\frac{a}{W}\leqslant 1. \tag{4}$$

This result is believed to be accurate to within one percent over the entire range of a/W. The results of Suresh et al. [4] determined for a specific choice of the other dimensional parameters of the finite geometry are in good agreement with (4).

Without loss of generality, the solution for the asymmetrically loaded specimen in Fig. 1 can be written as

$$K_{\mathrm{I}}=\frac{6(c-c_0)Q}{W^2}\sqrt{\pi a}F_{\mathrm{I}}(a/W) \tag{5a}$$

$$K_{\mathrm{II}}=\frac{\eta Q}{W^{1/2}}\frac{(a/W)^{3/2}}{(1-a/W)^{1/2}}F_{\mathrm{II}}(a/W) \tag{5b}$$

where, in general, c_0/W and η are functions of a/W, c/W, b_1/W, and b_2/W. The mode I stress intensity factor is not precisely zero where $M=0$, motivating the introduction of c_0. The representation (5) is chosen because it reduces to the reference solution ($c_0/W=0, \eta=1$) when the loading points are sufficiently far from the crack. The finite element results presented below indicate the reference solution is accurate to within about two percent as long as the distance of nearest loading point to the crack is greater than $1.4W$.

Figure 2 displays the dependence of c_0/W on a/W for three values of b_1/W and $\alpha\equiv(b_2-b_1)/W=1$. This was computed as the c/W at which $K_{\mathrm{I}}=0$. If the moment at the crack vanishes (i.e., $c=0$), the mode I factor can be significant when the loading points are near the crack. For example, for the extreme, but not entirely unrealistic case, where $b_1/W=0.6$, $\alpha=1$, $a/W=0.2$, and $c=0$, the mode mixity, $\psi=\tan^{-1}(K_{\mathrm{II}}/K_{\mathrm{I}})$, is 65 deg instead of 90 deg.

Variations of the mode II correction factor η with a/W for several c/W are shown in Fig. 3 for $b_1/W=1.0$ and $\alpha=1$. The error is largest for short cracks and for cracks on the order of a distance W from the closest loading point. Curves corresponding to constant values of the correction factor are plotted in Fig. 4, with $c/W=0.2$ and $\alpha=1$. If the combination ($b_1/W, a/W$) lies above the curve, the correction factor will be smaller than the corresponding η.

Finally, the effect of the parameter $\alpha=(b_2-b_1)/W$ is displayed in Fig. 5 by normalizing each of the respective stress intensity factors by the reference value from (2). These results have been computed with $b_1/W=1.4$ and $c/W=0.2$. The error in the reference values is less than roughly 2 percent when $\alpha>0.5$.

The plots in Figs. 2–5 provide guidance for either: (i) ensuring the test parameters are such that the reference solution (2) can be used with confidence, or (ii) estimating the corrections to the reference solution using (5). As long as the distance between the crack and the nearest loading point is greater than about $1.4W$

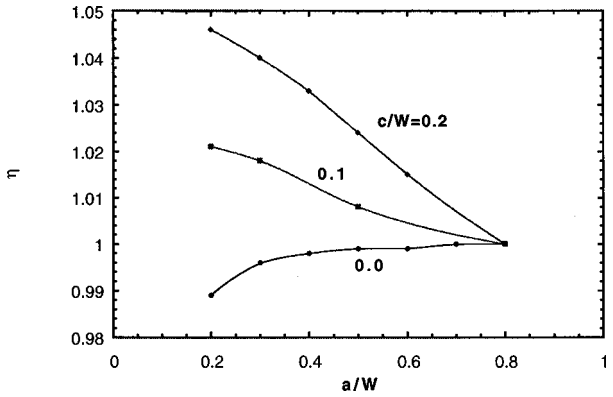

Fig. 3 Correction factor for mode II intensity factor ($\alpha=1$)

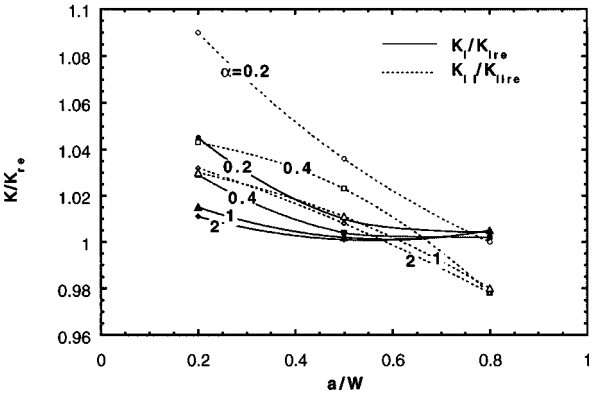

Fig. 5 Role of $\alpha=(b_2-b_1)/W$ in error of the reference solution (2) for $b_1/W=1.4$ and $c/W=0.2$

(i.e., $(b_1-c)/W>1.4$ with $b_2>b_1$) the reference solution is accurate to within a few percent. The errors in the reference solution are the smallest for deep cracks, i.e., $a/W\geqslant 0.5$.

Acknowledgment

This work was supported in part by the Multi-University Research Initiative on ''High Cycle Fatigue,'' which is funded at Harvard by AFSOR under Grant No. SA1542-22500 PG, and in part by the Division of Engineering and Applied Sciences, Harvard University.

References

[1] Campbell, J. P., 1998, private communication, University of California, Berkeley.

[2] Wang, K. J., Hsu, C. L., and Kao, H., 1977, ''Calculation of Stress Intensity Factors for Combined Mode Bend Specimens,'' *Advances in Research on the Strength and Fracture of Materials*, Vol. 4, D. M. R. Taplin, ed., ICF4, Waterloo, Canada, Pergamon Press, New York, pp. 123–133.

[3] He, M. Y., Cao, H. C., and Evans, A. G., 1990, ''Mixed-Mode Fracture: The Four-Point Shear Specimen,'' Acta Metall. Mater., **38**, pp. 839–846.

[4] Suresh, S., Shih, C. F., Morrone, A., and O'Dowd, N. P., 1990, ''Mixed-Mode Fracture Toughness of Ceramic Materials,'' J. Am. Ceram. Soc., **73**, pp. 1257–1267.

[5] Timoshenko, S. P., and Goodier, J. N., 1970, *Theory of Elasticity*, 3rd Ed. McGraw-Hill, New York.

[6] Tada, H., Paris, P. C., and Irwin, G. R., 1985, *The Stress Analysis of Cracks Handbook*, Del Research Corp., St. Louis, MO.

[7] Murakami, Y., 1987, *Stress Intensity Factors Handbook*, Pergamon Press, New York.

Large Shearing of a Prestressed Tube

M. Zidi

Université Paris 12 Val de Marne, Faculté des Sciences et Technologie, CNRS ESA 7052, Laboratoire de Mécanique Physique, 61, avenue du Général De Gaulle, 94010 Creteil Cedex, France
e-mail: zidi@univ-paris.12.fr

This study is devoted to a prestressed and hyperelastic tube representing a vascular graft subjected to combined deformations. The analysis is carried out for a neo-Hookean response augmented with unidirectional reinforcing that is characterized by a single additional constitutive parameter for strength of reinforcement. It is shown that the stress gradients can be reduced in presence of prestress. [S0021-8936(00)00101-X]

1 Introduction

Mechanical properties are of major importance when selecting a material for the fabrication of small vascular prostheses. The operation and the handing of prostheses vessel by surgeons, on the one part, the design of such grafts, on the other, induce specific loading and particularly boundary or initial conditions. Consequently, the interest in developing a theoretical model to describe the behavior of the prostheses vessel is proved ([1]). In this paper, we consider a thick-walled prestressed tube, hyperelastic, transversely isotropic, and incompressible assimilated to a vessel graft. We give an exact solution of the stress distributions when the tube is subjected to the simultaneous extension, inflation, torsion, azimuthal, and telescopic shears ([2–10]). The first theoretical results, in the case of a silicone tube, indicate that the increase of prestress minimizes the stress gradients due to the effects of the shear.

Contributed by the Applied Mechanics Division of THE AMERICAN SOCIETY OF MECHANICAL ENGINEERS for publication in the ASME JOURNAL OF APPLIED MECHANICS. Manuscript received by the ASME Applied Mechanics Division, Mar. 24, 1998; final revision, Oct. 12, 1999. Associate Technical Editor: M. M. Carroll.

2 Model Formulation

Consider a nonlinearly elastic opened tube defined by the angle ω_0 (Fig. 1). Let us suppose that the tube undergoes two successive deformations; first, including the closure of the tube which induced residual strains ([11]) and second, including inflation, extension, torsion, azimuthal and telescopic shears. The mapping is described by

$$r=r(R)\quad \theta=\left(\frac{\pi}{\omega_0}\right)\omega+\phi\alpha Z+\Theta(r)\quad z=\lambda\alpha Z+\Delta(r) \tag{1}$$

where (R,ω,Z) and (r,θ,z) are, respectively, the reference and the deformed positions of a material particle in a cylindrical system. ϕ is a twist angle per unloaded length, α and λ are stretch ratios (respectively, for the first and the second deformation), Θ is an angle which defined the azimuthal shear, and Δ is an axial displacement which defined the telescopic shear.

It follows from (1) that the physical components of the deformation gradient $\mathbf{F}$ has the following representation in a cylindrical system:

$$\mathbf{F}=\begin{bmatrix} \dot{r}(R) & 0 & 0 \\ r(R)\dot{\Theta}(r)\dot{r}(R) & \dfrac{r(R)}{R}\dfrac{\pi}{\omega_0} & r\phi\alpha \\ \dot{\Delta}(r)\dot{r}(R) & 0 & \alpha\lambda \end{bmatrix} \tag{2}$$

where the dot denotes the differentiation with respect to the argument.

Incompressibility then requires that $J\equiv\det\mathbf{F}=1$, which upon integration yields

$$r^2=r_i^2+\frac{\omega_0}{\pi\alpha\lambda}(R^2-R_i^2) \tag{3}$$

where R_i and r_i are, respectively, the inner surfaces of the tube in the free and in the loaded configurations (R_e and r_e are the outer surfaces).

The strain energy density per unit undeformed volume for an elastic material, which is locally and transversely isotropic about the $\mathbf{t}(R)$ direction, is given by

$$W=W(I_1,I_2,I_3,I_4,I_5) \tag{4}$$

where

$$I_1=Tr\mathbf{C},\quad I_2=\tfrac{1}{2}[(Tr\mathbf{C})^2-Tr\mathbf{C}^2],\quad I_3=1,$$
$$I_4=\mathbf{tCt},\quad I_5=\mathbf{tC}^2\mathbf{t} \tag{5}$$

are the principal invariants of $\mathbf{C}=\overline{\mathbf{F}}\mathbf{F}$ which is the right Cauchy-Green deformation tensor ($\overline{\mathbf{F}}$ is the transpose of $\mathbf{F}$).

The corresponding response equation for the Cauchy stress σ for transversely isotropic incompressible is (see [12])

$$\sigma=-p\mathbf{1}+2[W_1\mathbf{B}-W_2\mathbf{B}^{-1}+I_4W_4\mathbf{T}\otimes\mathbf{T}$$
$$+\mathbf{I}_4W_5(\mathbf{T}\otimes\mathbf{B}\cdot\mathbf{T}+\mathbf{T}\cdot\mathbf{B}\otimes\mathbf{T})] \tag{6}$$

where $\mathbf{B}=\mathbf{F}\overline{\mathbf{F}}$ is the left Cauchy-Green tensor, $\mathbf{1}$ the unit tensor, and p the unknown hydrostatic pressure associated with the incompressibility constraint, $W_i=(\partial W/\partial I_i)$ $(i=1,2,4,5)$ and $\mathbf{T}=(1/\sqrt{I_4})\mathbf{Ft}$.

From (6), the equilibrium equations in the absence of body forces are reduced to

$$\frac{d\sigma_{rr}}{dr}+\frac{\sigma_{rr}-\sigma_{\theta\theta}}{r}=0 \tag{7a}$$

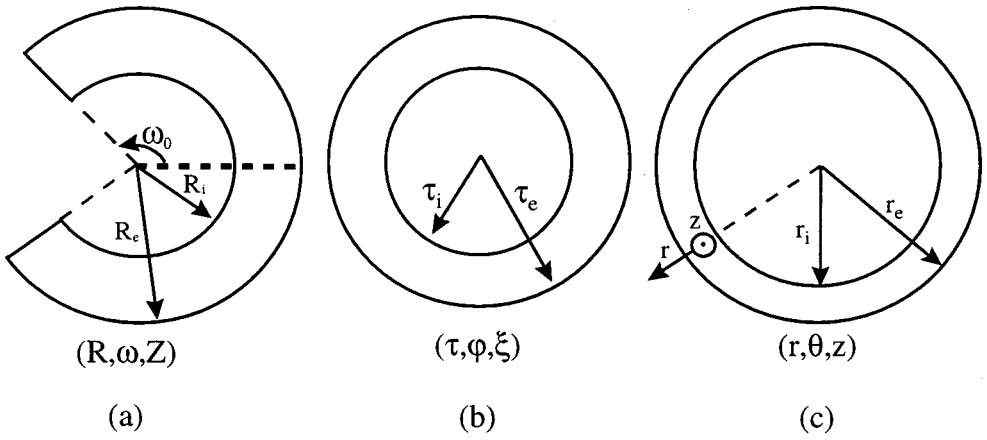

Fig. 1 Cross section of the tube in the stress-free (*a*), unloaded (*b*), and loaded configuration (*c*)

$$\frac{d\sigma_{r\theta}}{dr}+\frac{2\sigma_{r\theta}}{r}=0 \tag{7b}$$

$$\frac{d\sigma_{rz}}{dr}+\frac{\sigma_{rz}}{r}=0. \tag{7c}$$

Suppose that Θ and Δ satisfy the following boundary conditions: (a) $\Theta=\Theta_i$, $\Delta=\Delta_i$ in $r=r_i$ and (b) $\Theta=\Theta_e$, $\Delta=\Delta_e$ in $r=r_e$. Then, a simple computation by integrating (7*b*) and (7*c*) gives the expression of Θ and Δ.

Integrating (7*a*), given the boundary conditions that $\sigma_{rr}(r_i)=-p_i$ and $\sigma_{rr}(r_e)=0$, and taking $\mathbf{t}(R)=t_\omega(R)\mathbf{e}_\omega+t_Z(R)\mathbf{e}_Z$ and using (3) yields the pressure field p:

$$p(r)=p_i+2W_1\left(\frac{R\omega_0}{r\pi\alpha\lambda}\right)^2-2W_2 f(r)+\int_{r_i}^{r}\frac{\sigma_{rr}-\sigma_{\theta\theta}}{s}ds \tag{8a}$$

where

$$f(r)=\dot{\Delta}^2(r)\left[\frac{1}{(\alpha\lambda)^2}+\left(\frac{R\omega_0\phi}{\pi\lambda}\right)^2\right]+\dot{\Theta}^2(r)\left(\frac{R\omega_0}{\pi}\right)^2-2\frac{\dot{\Theta}(r)\dot{\Delta}(r)\phi\omega_0^2}{\alpha\pi}+\left(\frac{r\pi\alpha\lambda}{R\omega_0}\right)^2. \tag{8b}$$

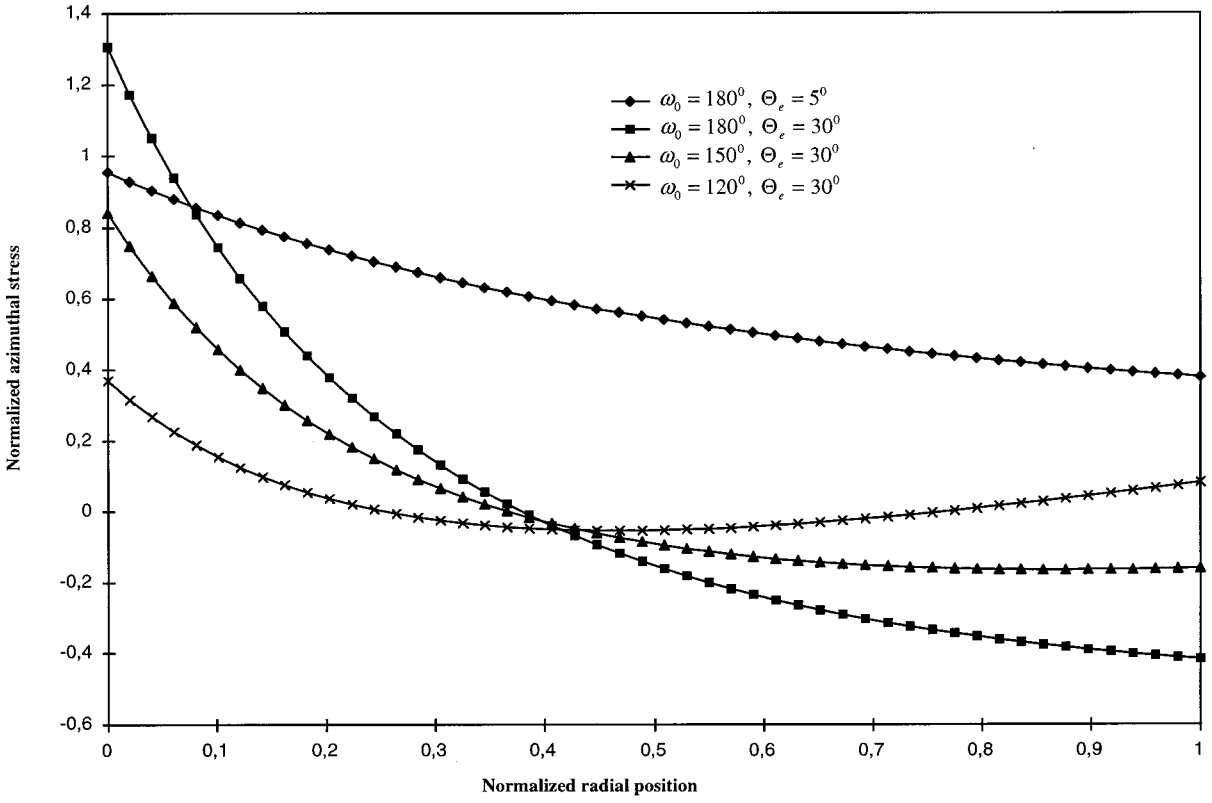

Fig. 2 Azimuthal stresses distribution inside the wall without fibers (stresses normalized by $\sigma_{r\theta}(r_e)$, $\mu=0.166$ Mpa, $p_i=0.0133$ Mpa, $\tau_i=2$ mm, $\tau_e=3$ mm)

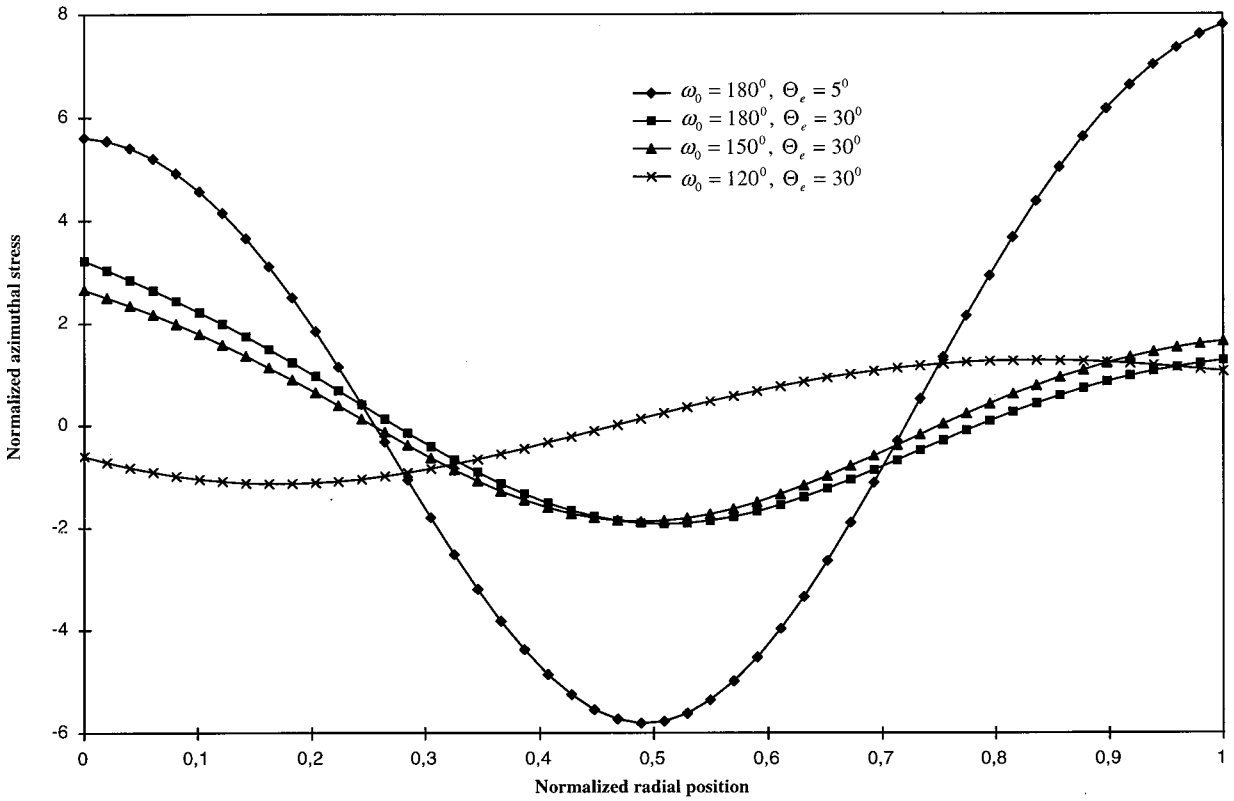

Fig. 3 Azimuthal stresses distribution inside the wall with fibers (stresses normalized by $\sigma_{r\theta}(r_e)$, $\mu = 0.166$ Mpa, $E_f = 10$ Mpa, $p_i = 0.0133$ Mpa, $\tau_i = 2$ mm, $\tau_e = 3$ mm)

The expressions of Θ, Δ, and p determine all the components of the Cauchy stress tensor σ.

3 Results

To illustrate the response of the proposed model, we use the extended Mooney Rivlin strain energy function which represents the behavior of a prosthesis ([13]) constituted of a silicone matrix and textile fibers,

$$W = W(I_1, I_4) = \frac{\mu}{2}(I_1 - 3) + \frac{E_f}{8}(I_4 - 1)^2, \tag{9}$$

where μ is the shear modulus of the isotropic matrix at infinitesimal deformations and E_f is the elastic modulus of the fibers.

The local tangent vector of the fibers is chosen here as $\mathbf{t}(R) = \cos\gamma(R)\mathbf{e}_\omega + \sin\gamma(R)\mathbf{e}_Z$ that represent a helical distribution of fibers ([1]).

From Eqs. (7*b*), (7*c*) and using (3) it easily follows that the expressions of Θ and Δ are

$$\Theta(r) = (\Theta_e - \Theta_i)\frac{\log\left[\dfrac{r}{r_i\sqrt{1 + k(r^2 - r_i^2)}}\right]}{\log\left[\dfrac{r_e}{r_i\sqrt{1 + k(r_e^2 - r_i^2)}}\right]} + \Theta_i \tag{10}$$

$$\Delta(r) = (\Delta_e - \Delta_i)\frac{\log[1 + k(r^2 - r_i^2)]}{\log[1 + k(r_e^2 - r_i^2)]} + \Delta_i \tag{11}$$

where $k = \pi\alpha\lambda/R_i^2\omega_0$.

As an illustrative result, we focus our attention only when the tube is submitted to azimuthal shear strain. Figure 2 shows the distribution of circumferential stresses generated by applied external azimuthal strain at a given pressure when taking into account the effects of such residual stresses. We show clearly that a decrease in ω_0 angle helps to distribute stresses in the loaded state when the shear is important. This result does not change qualitatively when varying the pressure p_i.

Furthermore, the particular effects of the presence of fibers have been examined with a linear distribution of fiber orientation within the data range $\gamma(R_i) = -40$ deg and $\gamma(R_e) = 40$ deg. As illustrated in Fig. 3, it is shown here that the effects of the azimuthal shear upon the distribution of the circumferential stresses within the wall become significant. When the tube is prestressed, the stresses are also distributed. Clearly these results will be able to help the design and fabrication of a small vascular prosthesis ([1]).

References

[1] How, T. V., Guidoin, R., and Young, S. K., 1992, ''Engineering Design of Vascular Prostheses,'' J. Eng. Med., **206**, Part H, pp. 61–71.

[2] Ogden, R. W., Chadwick, P., and Haddon, E. W., 1973, ''Combined Axial and Torsional Shear of a Tube of Incompressible Isotropic Elastic Material,'' Q. J. Mech. Appl. Math., **24**, pp. 23–41.

[3] Mioduchowski, A., and Haddow, J. B., 1979, ''Combined Torsional and Telescopic Shear of a Compressible Hyperelastic Tube,'' ASME J. Appl. Mech., **46**, pp. 223–226.

[4] Abeyaratne, R. C., 1981, ''Discontinuous Deformation Gradients in the Finite Twisting of an Incompressible Elastic Tube,'' J. Elast., **11**, pp. 43–80.

[5] Rajagopal, K. R., and Wineman, A. S., 1985, ''New Exact Solutions in Nonlinear Elasticity,'' Int. J. Eng. Sci., **23**, No. 2, pp. 217–234.

[6] Antman, S. S., and Heng, G. Z., 1984, ''Large Shearing Oscillations of Incompressible Nonlinearly Elastic Bodies,'' J. Elast., **14**, pp. 249–262.

[7] Simmonds, J. G., and Warne, P., 1992, ''Azimuthal Shear of Compressible or Incompressible, Nonlinearly Elastic Polar Orthotropic Tubes of Infinite Extant,'' Int. J. Non-Linear Mech., **27**, No. 3, pp. 447–467.

[8] Tao, L., Rajagopal, K. R., and Wineman, A. S., 1992, ''Circular Shearing and Torsion of Generalized Neo-Hookean Materials,'' IMA J. Appl. Math., **48**, pp. 23–37.

[9] Polignone, D. A., and Horgan, C. O., 1994, ''Pure Azimuthal Shear of

Compressible Nonlinearly Elastic Tubes,'' Q. Appl. Math., **50**, pp. 113–131.
[10] Wineman, A. S., and Waldron, W. K., Jr., 1995, ''Normal Stress Effects Induced During Circular Shear of a Compressible Nonlinear Elastic Cylinder,'' Int. J. Non-Linear Mech., **30**, No. 3, pp. 323–339.
[11] Sensening, C. B., 1965, ''Nonlinear Theory for the Deformation of Prestressed Circular Plates and Rings,'' Commun. Pure Appl. Math., **XVIII**, pp. 147–161.
[12] Spencer, A. J. M., 1984, *Continuum Theory of the Mechanics of Fibre-Reinforced Composites*, Springer-Verlag, New York.
[13] Cheref, M., Zidi, M., and Oddou, C., 1995, ''Caractérisation du Comportement Mécanique d'une Structure Polymérique: Aide à la Conception de Prothèses Vascularies,'' Arch. Physiol. Biochem., **103**, p. C63.

Buckling of a Short Cylindrical Shell Surrounded by an Elastic Medium

S. Naili
e-mail: naili@univ-paris12.fr

C. Oddou
e-mail: oddou@univ-paris12.fr

Laboratoire de Mécanique Physique, UPRES-A CNRS 7052, Université Paris XII, Val de Marne, Faculté des Sciences et Technologie, 61, avenue du Général de Gaulle, 94010 Créteil Cedex, France

The lateral surface of a cylindrical structure, which is composed of a thin tube embedded in a large outer medium, is submitted to a uniform external pressure. The buckling pressure of such a structure, corresponding to a low flexural state of the inner tube wall, is theoretically analyzed on the basis of the asymptotic method. The theoretical results are compared with experimental ones obtained from a compression test realized on an elastic tube inserted in a foam. It is found that the Euler pressure and the associated buckling mode index strongly depend upon the rheological and geometrical parameters of both the tube and the surrounding medium. [S0021-8936(00)00201-4]

1 Formulation of the Problem and Buckling Study

A nonhomogeneous cylindrical structure composed of a thin shell inserted in a surrounding elastic medium was subjected to a state of plane strain by external pressurization and zero axial longitudinal displacement constraint. The onset of the buckling process for such a structure was analyzed. The theoretical results were compared with original experimental ones as derived from a hoop compression test which was conducted with elastic rubber tubes embedded in foamy materials.

Thus, we consider the mechanical behavior of a cylindrical nonhomogeneous structure made of an internal shell confined in a large outer medium, the whole structure being submitted to a uniform pressure p on its external lateral surface. Each solid is elastic, cylindrical—of same axis—with a circular cross section in the reference configuration. In this configuration, the mean radius of the shell is denoted as r_0. The outer radius r_∞ of the medium is assumed to be very large compared to r_0. We will denote as e_0 the thickness of the shell. The two solids have the same height which is small in comparison with r_∞. The outer lateral boundary of the medium is subjected to a uniform pressure p. We assume frictionless contact between the two tubes. Body forces and inertia effects are deemed to be negligibly small.

The work of Forrestal and Herrman [1] presents solutions for both bonded and smooth conditions at the shell-medium interface; it includes a geometrically nonlinear formulation for both the shell and the medium. Moore and Booker [2] presented the linear approximation of Forrestal and Herrman's formulation. The physical unknowns which are involved in these theoretical formulations are the buckling pressure of the shell in the first work and the hoop compression stress inside this shell in the second one.

In the present work, we use the dimensionless buckling pressure of the overall structure consisting of the shell and surrounding medium developed by Razakamiadana et al. [3] and which is given by the relation

$$\bar{p}=n^2-1+\frac{\bar{\beta}}{n^2-1}, \tag{1}$$

where the dimensionless variables are given as follows:

$$\bar{p}=\alpha p\frac{r_0^3}{D},\quad \bar{\beta}=\beta\frac{r_0^4}{d},$$

and where $D=E_1e_0^3/12(1-\nu_1^2)$ is the flexural rigidity modulus of the shell, E_1 and ν_1 being, respectively, its Young's modulus and its Poisson's ratio, while the index n characterizes the buckling mode. The parameters α and β are defined by

$$\alpha=\frac{\left[\frac{\lambda_2+2\mu_2}{\lambda_2+\mu_2}\right]\left(2\frac{e_0}{r_0}\right)}{1-\left(1-2\frac{e_0}{r_0}\right)\left[1-\frac{\mu_2}{\mu_1}\right]+\frac{\mu_2}{\lambda_1+\mu_1}},$$

$$\beta=2\frac{\mu_2}{r_0}(\lambda_2+\mu_2)\left[\frac{n^2-1}{n(\lambda_2+2\mu_2)+\mu_2}\right],$$

in which the Lame's parameters of the shell and of the medium are denoted by λ_1,μ_1 and λ_2,μ_2, respectively.

In this study, we were interested in the smallest value of the buckling pressure—the Euler pressure—, while varying the index n associated with the buckling mode; such a mode index characterizes the number of axes of symmetry in the actual configuration. Indeed, this minimal pressure is the most frequently observed experimentally while applying incremental loading to the structure. This pressure is expressed as

$$p_e=\min_{n\geq 2}\left[\frac{1}{\alpha}\left((n^2-1)\frac{D}{r_0^3}+\frac{\beta r_0}{n^2-1}\right)\right]. \tag{2}$$

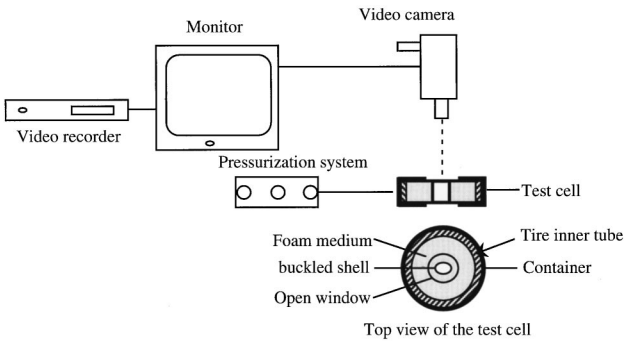

Fig. 1 Experimental apparatus for hoop compression tests. The tube inserted in the foam medium is in a buckled state with index of buckling mode equal to two.

Contributed by the Applied Mechanics Division of THE AMERICAN SOCIETY OF MECHANICAL ENGINEERS for publication in the ASME JOURNAL OF APPLIED MECHANICS. Manuscript received by the ASME Applied Mechanics Division, Feb. 12, 1999; final revision, July 22, 1999. Associate Technical Editor: S. Kyriadides.

Table 1 Experimental and theoretical results of Euler pressure normalized by E_2 and index of buckling mode n associated for various dimensionless mechanical and geometrical parameters

		Experiment				Theory	
$\overline{E}$	E_2 (kPa)	$\overline{e}$	e_0 (mm)	$p_e/E_2\times10^{-2}$	n	$p_e/E_2\times10^{-2}$	n
14.50	100	0.078	1.00	(8.69±0.80)	6	8.39	6
14.50	100	0.189	2.40	(15.34±2.19)	2	13.00	2
26.07	79	0.037	0.46	(4.21±0.40)	4	4.21	6
28.70	100	0.105	1.30	(11.00±1.00)	4	9.80	4
28.70	100	0.136	1.75	(12.89±0.92)	3	12.05	3
28.86	79	0.032	0.40	(3.98±0.33)	3	4.87	6
28.86	79	0.070	0.90	(6.13±0.63)	2	7.65	5
29.85	69	0.037	0.46	(4.66±0.78)	4	5.24	6
33.00	69	0.032	0.40	(4.21±0.21)	3	4.79	6
33.00	69	0.070	0.90	(6.10±0.31)	2	7.69	5
158.46	13	0.037	0.46	(11.76±3.69)	3	7.60	3
175.38	13	0.070	0.90	(17.69±0.10)	2	9.61	2

It is to be noted here that a classical case corresponds to the particular condition of an external incompressible fluid—i.e., $\mu_2=0$ and $\lambda_2\to\infty$—surrounding the shell, so that $\alpha=1$ and $\beta=0$ in relations (1) and (2).

2 Experimental Procedure

Hoop compression tests were performed on a cylindrical structure with a circular cross section composed by a thin rubber shell, of external radius $r_e=13$ mm which was inserted in a large foam medium of external radius $r_\infty=110$ mm. Both tubes had a height $H=30$ mm. The thin rubber shell was slightly stressed when inserted within the foam medium in order to establish a good contact between the two solids.

A steady loading was applied on the external lateral wall of the surrounding foam medium by means of a tire inner tube connected to a standard pressurization system. The plane strain of the structure was obtained by maintaining it between two circular and polished PMMA transparent plates. In order to avoid significant friction between the foam and the plates, the lower and upper faces of the foam were sprinkled with talc powder.

The applied pressure was measured by using a mercury *U*-manometer graded every 1 mm in height with a maximum reading error estimated at about 0.5 mm. When the buckling pressure is ''very low,'' the relative accuracy of the pressure measurement was estimated at about seven percent. But, in 90 percent of the cases, the measured pressure was about 50 mm Hg and the relative uncertainty of measurement was estimated, on average, to be one percent.

With this experimental setup, several tests of compression were conducted on the structure with given geometrical and mechanical characteristics. The tested structure was submitted to a gradual and slow loading so that, for each step, the system can be considered in stationary equilibrium state. The shape of the cross section of the shell remains circular before undergoing a change of shape. We monitored the evolution of shape with a CCD camera video placed on the axis of the tubes—see Fig. 1.

The thickness e_0 of the shell, in its reference configuration, was inferred from the mean value of the measurements conducted with a micrometer at various locations on the wall. The variations around the mean value were found to be in the order of two percent. The values of Young's modulus of the shell and of the medium were derived from traction and compression tests, respectively applied on samples of the constitutive materials. In the different experimental setup, four types of latex foam media with different Young's modulus and Poisson's ratio were combined with tubes made of various PCP, PCV, or latex materials having different characteristic mechanical properties as indicated in Table 1. For the deformations up to ten percent each Young's modulus was evaluated with a maximum error of five percent. Besides, these tests have shown that the Poisson's ratio of the shell was about 0.5—, i.e., the material is incompressible—whereas the Poisson's ratio for the foam media were around zero.

Next, the video images were digitized and then automatically processed using a global thresholding method so as to quantify the inner cross section area of the inserted tube and to characterize its shape. In the extreme case corresponding to a significant variation of this shape, the relative uncertainty of area measurement was estimated to be of the order of two percent. Indeed, when the structure is submitted to a gradual and slow loading, we retained as Euler pressure p_e, the one which corresponds to a clear change in the inner cross section area, as discussed later on.

For a given structure, the measurement of the buckling pressure was repeated ten times at least and the relative gap compared to the mean value varies between 1 percent and 30 percent.

3 Analysis and Discussion

We show, in columns 5 and 6 of Table 1, the experimental results obtained on 110 tests implying 12 structures of different geometry and elastic properties. The results are discussed by using the dimensionless geometrical and mechanical parameters $\overline{e}=e_0/r_0$ and $\overline{E}=E_1/E_2$ in the case of rather thin tubes and exter-

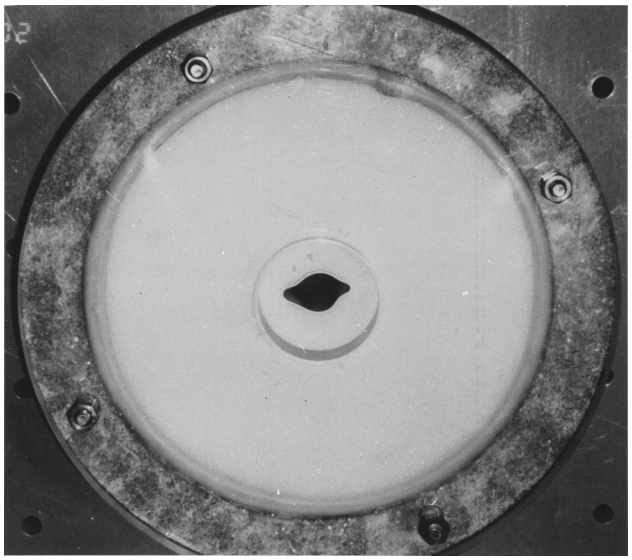

Fig. 2 Top view of the test cell giving an illustrative example of the tube inserted in the foam medium in a buckled state with index of buckling mode equal to four. Circular windows—with a radius in the order 30 mm—were cut on the top and bottom of the PPMA container for a better definition of the image during the recording.

nal foamy material softer than the rubbery one of the tube. Starting with Eq. (2), we determined the variations of the Euler pressure p_e normalized by E_2—denoted as $\overline{p_e}$—as a function of $\overline{E}$ for various values of $\overline{e}$. The associated buckling mode index n then depends on $\overline{E}$. It is worth noting that the assessment of the buckling pressure in such an experiment was based on the variation of a global geometrical parameter such as the area of the internal cross section of the inserted shell—see Fig. 2. Other more sensitive parameters, related to the changes in local shape properties could, however, be envisaged but their quantification by an image-processing system would have been more difficult to implement.

In columns 7 and 8 of Table 1, the theoretical results are compared with experimental ones. These results show that the Euler pressures, evaluated theoretically and determined experimentally, agree well accounting for the inherent scatter in experimental measurements. Moreover, the mode index n associated with $\overline{p_e}$ coincides exactly for 50 percent of the cases. Nevertheless, it is worth emphasizing that significant differences arised in the case of very thin tubes for which the mode index are rather high, the large number of lobes being more sensitive to small heterogeneities in material property and geometry. Despite this, the observed experimental results are, in general, well reproduced by our theoretical model.

References

[1] Forrestal, M. J., and Herrmann, G., 1965, ''Buckling of a Long Cylinder Shell Surrounded by an Elastic Medium,'' Int. J. Solids Struct., **1**, pp. 297–309.

[2] Moore, I. D., and Booker, J. R., 1985, ''Simplified Theory for the Behavior of Buried Flexible Cylinders Under the Influence of Uniform Hoop Compression,'' Int. J. Solids Struct., **21**, No. 9, pp. 929–941.

[3] Razakamiadana, A., Naili, S., and Oddou, C., 1997, 'Flambement d'une Coque Mince Confinée : Théorie et Expérience,' C. R. Acad. Sci., Ser. IIb: Mec., Phys., Chim., Sci. Astron., **325**, pp. 119–126.

A Numerical Tool for Periodic Heterogeneous Media: Application to Interface in Al/SiC Composites

D. Dumont
Faculté de Mathématiques et d'Informatique, 33, rue Saint-Leu, 80 039 Amiens, France
e-mail: Serge.Dumont@u-picardie.fr

F. Lebon
Laboratoire de Mécanique et Génie Civil, Université Montpellier 2, Pl. E. Bataillon, 34 095 Montpellier Cedex 5, France
e-mail: lebon@lmgc.univ-montp2.fr

A. Ould Khaoua
Departamento de Matematicas, Universidad de los Andes, Calle 19 1-11, Bogota, Columbia
e-mail: ahmed@media.uniandes.edu.co

A wavelet-Galerkin method for periodic heterogeneous media is presented. The advantages are to remove the mesh and to make adaptivity easier. Numerical results are presented. A specific study of interfaces in a Al-SiC composite is given.

[S0021-8936(00)00301-9]

1 Introduction

A great number of recent papers are concerned by the solution of partial differential equations by wavelet bases ([1,2]). Mainly, these works deal with one-dimensional or scalar two-dimensional problems. The solution of the elastostatics system by this kind of method is not usual ([3,4]). Boundary problems on open bounded sets are very difficult to treat ([5]). Nevertheless, periodic conditions on elementary bounded sets are natural for the use of wavelet transform. In this paper, we show how to use such a technique and we give applications to interfaces in Al-SiC composite. In the first section we give the notations and the necessary mathematical background. In the second section we present the mechanical problem: the homogenization of periodic heterogeneous media. The third section is concerned with the algorithm: a wavelet-Galerkin method using Daubechies wavelets ([6]). The determination of the macroscopic coefficients is treated in the fourth section. Applications and numerical results are described in the fifth section. Concluding remarks are given.

2 Notations and Mathematical Background

In this section, we present the notations used in the following of the paper. The sets of kinematically and statically admissible fields are denoted H, L, and S. Let

$$L=(L^2(Y))^3 \quad \text{and} \quad H=(H_p^1(Y))^2$$

$$S=\{v\in L^2_{loc}(Y), v(x_1+k_1,x_2+k_2)=v(x_1,x_2)\text{a.e.},k_1,k_2\in\mathbb{K}\} \tag{1}$$

$$H_p^1(Y)=\{v\in S,\ v_{,i}\in L^2(Y),\ i=1,2\}.$$

$u_{,i}$ denotes the ith partial derivative of the function u. We denote C the fourth-order elasticity tensor, e the strain tensor, and σ the stress tensor. In the following $Y=]0,1[^2$. To construct a wavelet basis of H, we use the compactly supported wavelets introduced by I. Daubechies [6] which is a basis of $L^2(\mathbb{R})$. These wavelets are periodized in order to obtain bases of S. By tensorial and cartesian products wavelet bases of H are obtained ([7]). We denote Ψ^l, $l=1, 2, 3$, and Ψ^0 the wavelets and the scale functions (six degrees-of-freedom for each point), $N^j=2^j-1$ and $\Lambda^j=[0,N^j]^2$.

Let V_j be the subspace of dimension 2^{2j+1} of H generated by this wavelet at approximation level j. An element of $V_{j\,\max}$ is thus written as

$$u(x_1,x_2)=(u_1(x_1,x_2),u_2(x_1,x_2))$$

$$u_d=\sum_{\kappa\in\Lambda_{j_0}} u^{d0}_{j_0\kappa}\Psi^0_{j_0\kappa}+\sum_{l=1}^{l=3}\sum_{j=j_0}^{j=j\,\max}\sum_{\kappa\in\Lambda_j} u^{dl}_{j\kappa}\Psi^l_{j\kappa}. \tag{2}$$

j_0 is a given integer, $d=1$ or 2 and $\kappa=(k_1,k_2)$.

3 The Mechanical Problem

We consider a multiphase isotropic elastic composite (Fig. 1) and we intend to study the behavior of this heterogeneous media. We introduce the notion of equivalent material, i.e., we mean that under the same loadings, this equivalent material has globally the same response. In former papers ([8,9]) bounds for the bulk and shear moduli of a two-phase composite have been given. Without going into further detail, these bounds depend on the shear and bulk moduli of the two phases and on the volumic fraction of the two phases in the composite. In the same way, the theory of periodic homogenization ([10]) focuses on an idealized composite

Contributed by the Applied Mechanics Division of THE AMERICAN SOCIETY OF MECHANICAL ENGINEERS for publication in the ASME JOURNAL OF APPLIED MECHANICS. Manuscript received by the ASME Applied Mechanics Division, Mar. 15, 1999; final revision, Sept. 15, 1999. Associate Technical Editor: M. Ortiz.

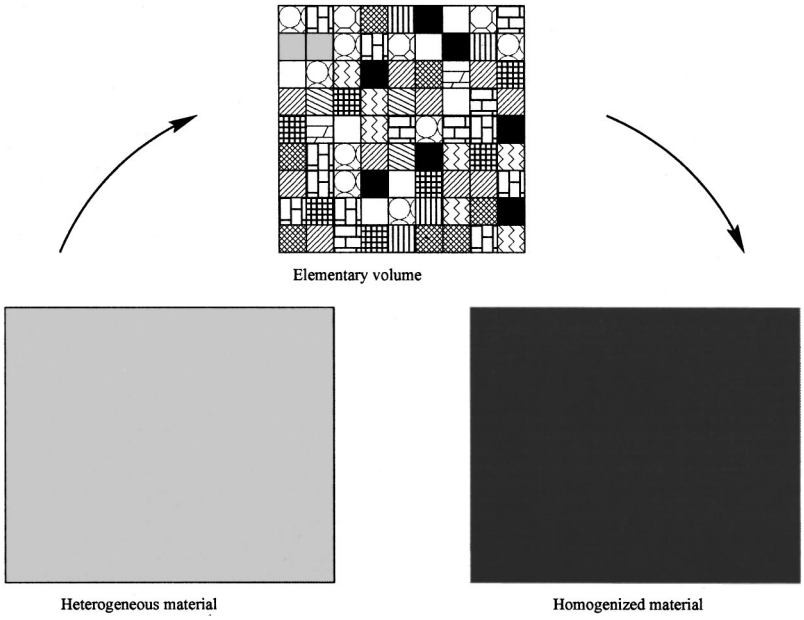

Fig. 1 An example of a composite and its representative volume

consisting of the juxtaposition of identical heterogeneities and classically, we need to solve an elastostatics problem on a representative volume Y (Problem P):

Problem. P

$E \in L$ be given, find $u \in H$ such that $a(u,v)=l(v)\ \forall v \in H$

$$\text{with } a(u,v)=\int_Y \sigma(u):e(v)dy=\int_Y C(y)e(u):e(v)dy$$

$$\text{and } l(v)=-\int_Y CE:D(v)dy$$

Because of the nonuniqueness of the solution of problem (P) (defined within a translation), problem (P) is replaced by problem (P_ε) (''viscous'' problem):

Problem. P_ε

$E \in L$ be given, find $u \in H$ such that $a_\varepsilon(u,v)=l(v)\ \forall v \in H$

$$\text{with } a_\varepsilon(u,v)=\int_Y \sigma(u):e(v)dy+\varepsilon\int_Y uvdy$$

It can be shown that the solution of this problem converges toward the solution of problem (P) with average equal to zero ([4]).

Remarks.

(i) The problem (P) is solved classically by a finite element method or by fast Fourier transform ([11]). We have chosen to introduce wavelet methods in order to eliminate the notion of mesh and to eliminate Gibbs phenomena.

(ii) If the discretization of problem (P) in a orthonormal wave-

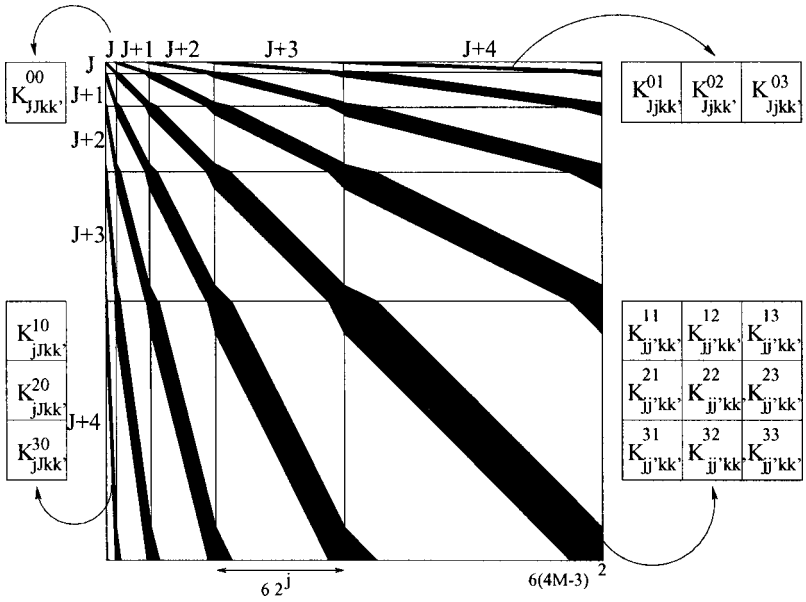

Fig. 2 Wavelet element matrix ($j_0=J$, $j_{max}=J+4$)

let basis leads to the system $KU=B$, then the discretization of problem (P_ε) leads to $(K+\varepsilon Id)U=B$, where Id is the identity matrix.

(iii) The tensor C could be given by the image (pixels) of the microstructure.

4 Wavelet-Galerkin Method

The variational problem (P_ε) is discretized by a Galerkin method. We have introduced a wavelet basis because of their localization and adaptivity properties. The projection of the plane elasticity operator into the wavelet basis ([7]) is given by a stiffness matrix K where the ''elementary matrix'' of order 2 is

$$K^{ll'}_{jj'\kappa\kappa'} = \begin{bmatrix} F_{1111}+F_{1321}+F_{3112}+F_{3322} & F_{1221}+F_{1311}+F_{3222}+F_{3312} \\ F_{1212}+F_{2322}+F_{3111}+F_{3321} & F_{2222}+F_{2312}+F_{3221}+F_{3311} \end{bmatrix} \tag{3}$$

where

$$F_{pq\alpha\beta}=\int_Y \mathbb{C}_{pq}\Psi^l_{j\kappa,\alpha}\Psi^{l'}_{j'\kappa',\beta}\,dx_1dx_2.$$

We have chosen to decompose the tensor C on a wavelet basis at level J noted θ. In the numerical applications, Haar wavelet is used with its compact support equal to the square $[l_1/2^j,(l_1+1)/2^j]\times[l_2/2^j,(l_2+1)/2^j]$. This wavelet is constant on this support which is a pixel of the image representation. Thus, the wavelet coefficient θ_{jl} is equal to the value of the tensor C on this pixel. Due to the form of the wavelets (Cartesian and tensorial products of one dimensional wavelets) the computation of the coefficients of the matrix K leads to the determination of elementary terms which are integral of products of three one-dimensional wavelets and their derivatives:

$$\int_0^1 \theta_{Jr}\frac{d^m\Psi_{js}}{dx^m}\frac{d^n\Psi_{jt}}{dx^n}, \quad m,n=0,1. \tag{4}$$

These terms are obtained by the determination of eigenvectors of a low-order matrix ([7,12]). The right-hand side of the problem corresponding to the term $l(v)$ in problem (P_ε) is computed by a similar technique ([4,5]). Classically, the matrix K is a sparse matrix (Fig. 2). Because of the form of the wavelets bases, it seems natural to solve the linear system which is a discretized version of problem (P_ε) by multigrid techniques ([13,14]). Nevertheless, we have chosen to use a conjugate gradient method.

5 Determination of the Macroscopic Coefficients

The determination of the elastic macroscopic coefficients corresponds to the computation of the macroscopic stress tensor Σ:

$$\Sigma=\int_Y (CE+Ce(u))dx_1dx_2. \tag{5}$$

The computation of these terms is in the same way as the matrix and the right-hand side [4].

6 Numerical Results

We present the example of a three-phase fiber-matrix composite (Fig. 3): SiC for the fiber, Al for the matrix and an interface. The Lamé coefficients associated to the interface are $\lambda\,\eta^\alpha$ and $\mu\,\eta^\beta$ where $\eta\gamma$ is the thickness of the interface. α and β are real positive parameters and γ is a given function with a sufficient regularity. We have shown in former papers ([15–17]) that when η tends to zero, i.e., the thickness and the rigidity parameters tend to zero, we obtain an elastostatic limit problem with an interface law. This interface law keeps in memory the mechanical and geometrical properties of the layer. The interface law is given in

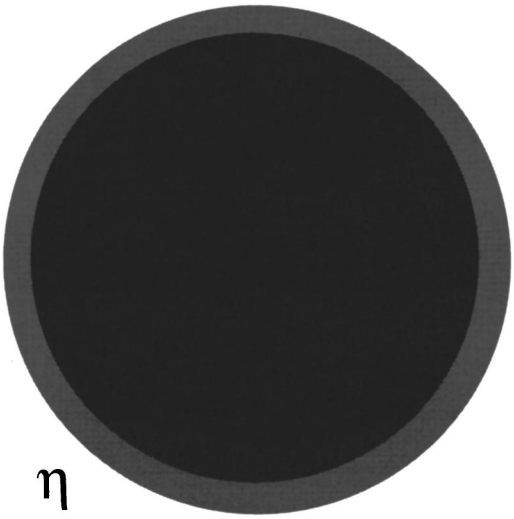

Fig. 3 Al-SiC composite with an interfacial zone (thickness η)

Table 1 Interface laws

$\mu/\epsilon\to 0$	$u_N=0\ \ \sigma_T=0$	$\sigma_N=\frac{\overline{\lambda}}{\gamma}u_N\ \ \sigma_T=0$	$\sigma_n=0$
$\mu/\epsilon\to\overline{\mu}$	$u_N=0\quad \sigma_T=\frac{\overline{\mu}}{\gamma}u_T$	$\sigma_N=\left(\frac{\overline{\mu}}{\gamma}+2\frac{\overline{\lambda}}{\gamma}\right)u_N$	$\sigma_N=2\frac{\overline{\lambda}}{\gamma}u_N$
		$\sigma_T=\frac{\overline{\mu}}{\gamma}u_T$	$\sigma_T=\frac{\overline{\mu}}{\gamma}u_T$
$\mu/\epsilon\to\infty$	$u=0$ $\lambda/\epsilon\to\infty$	$u=0$ $\lambda/\epsilon\to\overline{\lambda}$	$u=0$ $\lambda/\epsilon\to 0$

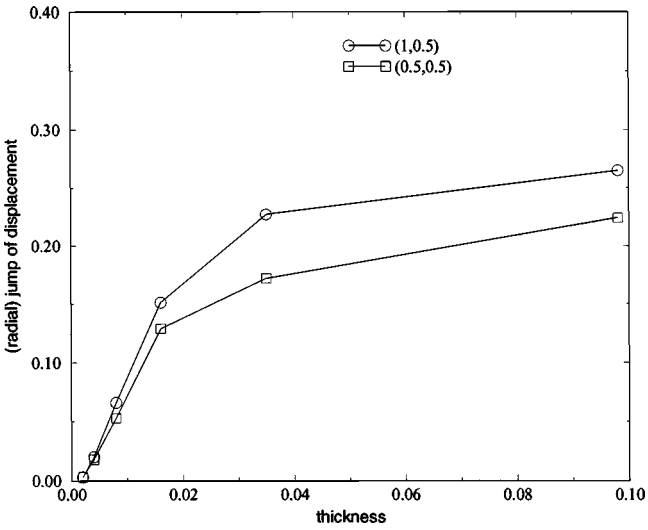

Fig. 4 Jump of displacement for different values of α and β ($M=3$)

Table 1 with respect to the value of the parameters α and β. α and β determine how the thickness and the rigidity tend to zero. It is necessary to quantify the limit, in other words we seek an interval in which the initial problem could be approximated by the limit problem for which the solution is more easy to obtain. On the other hand, it is very important to quantify the influence

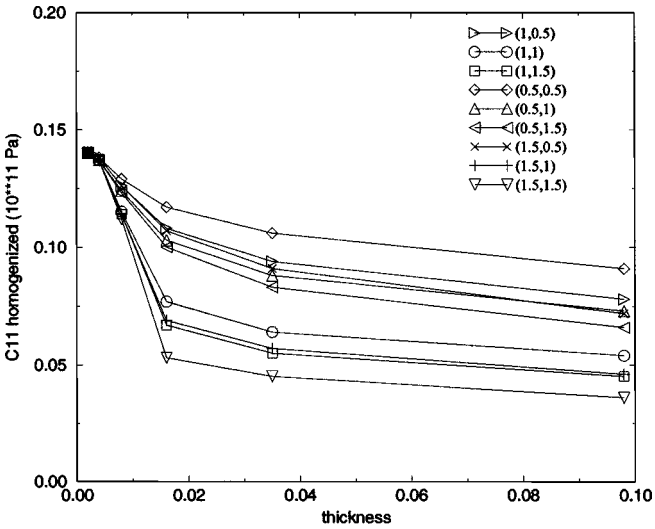

Fig. 5 Homogenized coefficient for different values of α and β ($M=3$)

of the interface on the macroscopic coefficients, i.e., on the elastic behavior of a structure. Due to the shape and the thickness of the interface this problem is very difficult to treat by classical techniques.

We present, in Fig. 4, a study of the convergence of the jump of displacement in the interface for the case $\gamma=1$, for two values of α and β. λ and μ are chosen as Aluminum coefficients. In this case the jump is equal to zero in the interface law. We have found that for values of η smaller than 0.4 p.c. of the structure the interface law could be considered as valid. Note that the displacement in the interface has the form ([16]) $u(r,\theta)\simeq ru(\theta)+u_0$. Figure 5 shows the influence of the thickness parameter on the first component of the homogenized elasticity tensor for different values of α and β. For small values of the thickness (η smaller than 0.2 p.c. of the structure) it is convenient to neglect the interface. Note that for values of the thickness larger than 0.02, the coefficient depends linearly on the thickness.

7 Concluding Remarks

In this paper, we have shown a robust tool to compute the overall response of a composite. In particular, our method is able to compute the influence of an interface even at a very small level. In the future, we want to investigate more complex materials such random materials ([18]) or other kind of interfaces ([19,20]).

References

[1] Charton, P., and Perrier, V., 1996, ''A Pseudo-Wavelet Scheme for the Two Dimensional Navier-Stokes Equation,'' Comp. Appl. Math., **15**, pp. 139–160.

[2] Lazaar, S., Ponenti, P. J., Liandrat, J., and Tchamitchian, P., 1994, ''Wavelet Algorithms for Numerical Resolution of Partial Differentiable Equations,'' Comput. Methods Appl. Mech. Eng., **116**, pp. 309–314.

[3] Dumont, S., 1996, ''Ondelettes, Homogénéisation Périodique et Elasticité,'' Ph.D. thesis, Université Montpellier 2.

[4] Dumont, S., and Lebon, F., 1996, ''Wavelet-Galerkin Method for Heterogeneous Media,'' Comput. Struct., **61**, pp. 55–65.

[5] Dumont, S., and Lebon, F., 1999, ''Wavelet-Galerkin Method for Plane Elasticity,'' Comp. Appl. Math., **18**, pp. 127–142.

[6] Daubechies, I., 1992, ''Orthonormal Bases of Compactly Supported Wavelets,'' Commun. Pure Appl. Math., **41**, pp. 909–998.

[7] Dumont, S., and Lebon, F., 1996, ''Representation of Plane Elastostatics Operators in Daubechies Wavelets,'' Comput. Struct., **60**, pp. 561–569.

[8] Hashin, Z., and Strickman, S., 1963, ''A Variational Approach to the Theory of the Elastic Behavior of Multiphase Materials,'' J. Mech. Phys. Solids, **11**, pp. 127–140.

[9] Hill, R., 1964, ''Theory of Mechanical Properties of Fiber-Strenghened Materials,'' J. Mech. Phys. Solids, **12**, pp. 199–212.

[10] Bensoussan, A., Lions, J. L., and Papanicolaou, G., 1978, *Asymptotic Analysis for Periodic Structures*, 1st Ed., North-Holland, Amsterdam.

[11] Dumontet, H., 1983, ''Homogénéisation par Développement en Séries de Fourier,'' C. R. Acad. Sci. Paris, **296**, pp. 1625–1628.

[12] Beylkin, G., 1992, ''On the Representation of Operators in Bases of Compactly Supported Wavelets,'' SIAM (Soc. Ind. Appl. Math.) J. Numer. Anal., **29**, pp. 1716–1740.

[13] Hackbusch, W., 1985, *Multigrid Method and Applications*, Springer-Verlag, New York.

[14] Lebon, F., 1995, ''Two-Grid Method for Regularized Frictional Elastostatics Problems,'' Eng. Comput., **12**, pp. 657–664.

[15] Ould Khaoua, A., 1995, ''Etude Théorique et Numérique de Problèmes de Couches Minces,'' Ph.D. thesis, Université Montpellier 2.

[16] Ould Khaoua, A., Lebon, F., Licht, C., and Michaille, G., 1996, ''Thin Layers in Elasticity: A Theoretical and Numerical Study,'' *Proceedings of the 1996 ESDA Conference*, Vol. 4, ASME, New York, pp. 171–178.

[17] Lebon, F., Ould Khaoua, A., and Licht, C., 1997, ''Numerical Study of Soft Adhesively Bonded Joints in Finite Elasticity,'' Comp. Mech., **21**, pp. 134–140.

[18] Garboczi, E. J., and Bentz, D. P., 1991, ''Digital Simulation of Interfacial Packing in Concrete,'' J. Mater. Res., **6**, pp. 196–201.

[19] Hervé, E., and Zaoui, A., 1995, ''Elastic Behavior of Multiply Coated Fibre-Reinforced Composites,'' Int. J. Eng. Sci., **33**, pp. 1419–1433.

[20] Lagache, M., Agbossou, A., Pastor, J., and Muller, D., 1994, ''Role of Interphase on the Elastic Behavior of Composite Materials: Theoretical and Experimental Analysis,'' J. Compos. Mater., **28**, pp. 1140–1157.

On the Original Publication of the General Canonical Functional of Linear Elasticity

C. A. Felippa

Mem. ASME, Department of Aerospace Engineering and Center for Aerospace Structures, University of Colorado, Boulder, CO 80309-0429

The general canonical functional of linear elastostatics is associated with the names of Hu and Washizu, who published it independently in 1955. This note discusses how that functional, in a generalized four-field form, had been derived by B. M. Fraeijs de Veubeke in a 1951 technical report. This report presents five of the seven canonical functionals of elasticity. In addition to the general functional, it exhibits what is likely the first derivation of the strain-displacement dual of the Hellinger-Reissner functional. The tour of five variational principles takes only a relatively small portion of the report: 8 pages out of 56. The bulk is devoted to the use of energy methods for analysis of wing structures. The title, technology focus, and limited dissemination may account for the subsequent neglect of this original contribution to variational mechanics. [S0021-8936(00)00401-3]

Introduction

The three-field canonical functional of linear elastostatics, herein abbreviated to C3FLE, is identified as the Hu-Washizu functional in the mechanics literature. In this functional the three interior fields, displacements, stresses, and strains, are independently varied. The attribution is supported by two independent publications that appeared concurrently, in Mar. 1955 ([1,2]). A four-field generalization, in which surface tractions are independently varied, will be called C4FLE.

An expository article (actually a book chapter) by Fraeijs de Veubeke [3] is often cited as one of the early classics in the finite element literature. That article contains the first enunciation of the ''limitation principle,'' which has since served as guide in the construction of mixed elements. His exposition of variational

Contributed by the Applied Mechanics Division of THE AMERICAN SOCIETY OF MECHANICAL ENGINEERS for publication in the ASME JOURNAL OF APPLIED MECHANICS. Manuscript received by the ASME Applied Mechanics Division, Apr. 22, 1999; final revision, Oct. 12, 1999. Associate Technical Editor: M. Ortiz.

methods starts from the C4FLE functional, which he calls ''the general variational principle.'' However, it does not reference Hu and Washizu as its source but an earlier technical report, written in French ([4]). This appears as the third reference in the 1965 article.

A subsequent journal paper on variational principles, [5], is slightly more explicit. It begins: ''There is a functional that generates all the equations of linear elasticity theory in the form of variational derivatives and natural boundary conditions. Its original construction [12] followed the method proposed by Friedrichs . . . '' The reference number points to that report.

These references motivated the writer to investigate whether de Veubeke had indeed constructed that functional in the 1951 report. That would confer him priority over Hu and Washizu, although of course these two papers were more influential in subsequent work. The writer was able to procure an archived copy thanks to Profs. Beckers and Geradin of the University of Liège, where Fraeijs de Veubeke was a professor of aeronautical engineering from the early 1950s until his untimely death in 1977.

Construction of the C4FLE Functional

As discussed below, in the 1951 report Fraeijs de Veubeke constructs not simply the canonical three-field principle, but the four-field generalization C4FLE. Consequently his priority is established unless an earlier publication can be found. The functional, however, appears as an intermediate result on the road from the total potential energy (TPE) to the total complementary energy (TCE) principle. The path also traverses a pair of two-field functionals, one being a generalization of the Hellinger-Reissner (HR) functional published the previous year by Reissner [6]. The full sequence can be sketched as

$$\text{TPE}\rightarrow\text{C4FLE}\rightarrow\text{Strain-displacement dual of HR}\rightarrow\text{HR}\rightarrow\text{TCE}. \tag{1}$$

The report does not call special attention to C4FLE, as well as to the strain-displacement functional that appears there for the first time. The bulk of the material is indeed devoted to the study of energy-based approximation methods for the analysis of monocoque wing structures, rather than to the derivation of new functionals. Its title, technology focus, and target audience (structural engineers) are likely responsible for subsequent neglect. This is reinforced by its limited dissemination and the fact that the material was apparently not submitted to an archival journal.

Fraeijs de Veubeke uses the full-component notational form popularized by Timoshenko and others, which was then common in continuum mechanics. For historical accuracy this will be followed below until Eq. (10), at which point it is changed to modern indicial notation for compactness. The equations taken from the report have been sequentially renumbered.

The report comprises three chapters. The last two, which deal with the title application, are of no concern here. Chapter I begins by summarizing the field equations of linear elastostatics for a three-dimensional body of volume V and surface S. The fields in V are displacements u, v, w, body forces X, Y, Z, infinitesimal strains $\epsilon_x, \gamma_{xy}, \ldots, \epsilon_z$ and stresses $\sigma_x, \tau_{xy}, \ldots, \sigma_z$. The surface S is divided into S_1, on which tractions $\overline{p_x}$, $\overline{p_y}$, $\overline{p_z}$ are known,and S_2, on which displacements $\overline{u}$, $\overline{v}$, $\overline{w}$ are prescribed. The direction cosines of the exterior normal to S are denoted by l, m, n.

As starting point for the variational developments (Chapter I, p. 6) Fraeijs de Veubeke exhibits the TPE principle:

$$\delta\left[\int_V W\, dV + P_V + P_S\right] = 0. \tag{2}$$

Here W is the internal energy density in terms of displacements, whose first variation is

$$\delta W = \sigma_x \delta\frac{\partial u}{\partial x} + \tau_{xy}\delta\left(\frac{\partial u}{\partial y}+\frac{\partial v}{\partial x}\right) + \cdots + \sigma_z\delta\frac{\partial w}{\partial z} \tag{3}$$

and P_V and P_S are potentials of the body (volume) forces and surface tractions, respectively,

$$P_V = \int_V (\overline{X}u + \overline{Y}v + \overline{Z}w)\,dV \tag{4}$$

$$P_S = \int_{S_1} (\overline{p_x}u + \overline{p_y}v + \overline{p_z}w)\,dS. \tag{5}$$

Fraeijs de Veubeke presents the well-known Euler equations of the TPE principle. Next (on p. 8) he recasts the internal energy density in terms of strains: $W = W(\epsilon)$ so that the variation becomes

$$\delta W = \sigma_x\delta\epsilon_x + \tau_{xy}\delta\gamma_{xy} + \cdots + \sigma_z\delta\epsilon_z\,. \tag{6}$$

Following that he states that to free (''libérer'') strains from the strain-displacement constraints and the boundary displacements from the prescribed displacement constraints, one must add to the expressions to be varied the volume term

$$\int_V\left[T_{xx}\left(\frac{\partial u'}{\partial x}-\epsilon_x\right)+T_{xy}\left(\frac{\partial u'}{\partial y}+\frac{\partial v'}{\partial x}-\gamma_{xy}\right)+\cdots\right]dV \tag{7}$$

in which $(T_{xx}, T_{xy}, \ldots)$ are Lagrange multipliers in V, as well as the surface term

$$\int_{S_2}[\alpha_x(\overline{u}-u)+\alpha_y(\overline{v}-v)+\alpha_z(\overline{w}-w)]\,dS \tag{8}$$

in which $(\alpha_x, \alpha_y, \alpha_z)$ are multipliers on S_2. The displacements in (7) are marked by a prime to emphasize that the variations of the strains have become independent of the displacement gradients.

Fraeijs de Veubeke states on p. 9 that this expanded functional is subject to 18 independent variations: three displacements, six strains, six T multipliers, and three α multipliers. He had noted earlier (on p. 8) that variations with respect to the strains in V give as Euler equations

$$T_{xx} = \frac{\partial W}{\partial\epsilon_x}, \quad T_{xy} = \frac{\partial W}{\partial\gamma_{xy}}\ \ldots \tag{9}$$

whereas variations with respect to the displacements on S_2 give as Euler equations

$$\alpha_x = lT_{xx} + mT_{xy} + nT_{xz}, \ldots\,. \tag{10}$$

Hence the T multipliers form a stress system whereas the α multipliers form a system of surface tractions. Fraeijs de Veubeke denotes these as σ' and p' in later publications, such as the cited 1965 article.

Except for P_V and P_S, Fraeijs de Veubeke does not define global symbols to identify his integrals. For convenience we remedy that omission by calling $U_\epsilon = \int_V W(\epsilon)dV$ and identifying Eqs. (7) and (8) by D_V and D_S, respectively, where D stands for the term ''dislocation potential'' now in vogue. We can thereby collect all the pieces into one compact expression:

$$\delta[U_\epsilon + D_V + P_V + P_S + D_S] = 0. \tag{11}$$

The expression in brackets is the C4FLE functional, which in indicial notation can be compactly presented as

$$\Pi(u_i, \sigma_{ij}, \epsilon_{ij}, t_i) = \int_V [W(\epsilon_{ij}) + \sigma_{ij}(u_{(i,j)} - \epsilon_{ij}) - f_i u_i]dV - \int_{S_1}\overline{t_i}u_i dS - \int_{S_2} t_i(\overline{u_i}-u_i)dS \tag{12}$$

in which $u_{(i,j)}$ denotes the symmetric gradient of the displacement field. The three-field standard form C3FLE is obtained by setting $t_i = \sigma_{ij}n_j$ on S_2 a priori. A variant of C3FLE involving stress derivatives, displayed for example in Gurtin [7] follows from integration by parts.

A Strain-Displacement Functional

Continuing along the path (1), Fraeijs de Veubeke replaces the multipliers in (7) and (8) by (9) and (10), respectively, and exhibits on p. 9 a two-field functional in which strains and displacements are primary variables. His full form expression is fairly long. In indicial notation it becomes

$$\Pi(u_i,\epsilon_{ij}) = \int_V \left[W(\epsilon_{ij}) + \frac{\partial W}{\partial \epsilon_{ij}}(u_{(i,j)} - \epsilon_{ij}) - f_i u_i \right] dV - \int_{S_1} \overline{t}_i u_i dS - \int_{S_2} \frac{\partial W}{\partial \epsilon_{ij}} n_j (\overline{u}_i - u_i) dS \qquad (13)$$

in which for linear elasticity $\partial W/\partial \epsilon_{ij}$ is understood to be $E_{ijkl}\epsilon_{kl}$. Now (13) is the stress-strain dual of Hellinger-Reissner (HR) but has escaped a name.

In an expository article ([8]), the writer called it ''Strain-Displacement Reissner'' following Oden and Reddy [9] who labeled it a Reissner functional when constructed as a member of a canonical set of elasticity functionals ([10]). However, in a 1995 letter to the writer, Professor Reissner indicated that he had not considered that form. This functional has had little use in mechanics until assumed-strain finite elements began appearing in the 1980s.

Again, Fraeijs de Veubeke uses Eq. (13) only as an intermediate result. He applies a Friedrichs-style Legendre transformation to it and arrives on p. 10 at a generalized form of the Hellinger-Reissner (HR) functional. He remarks that it had been published by Reissner [6] but that the rederived form is slightly more general in that it includes body forces as well as prescribed nonzero displacements.

The remainder of Chapter I (pp. 11–18) is devoted to the derivation of the TCE functional from HR, and the energy theorems of Castigliano and Menabrea. Even for this better known material Fraeijs de Veubeke displays a mastery of variational techniques unusual for the times. For example, several textbooks still thoughtlessly lift Castigliano's second theorem $u_i = \partial U(\sigma)/\partial F_i$ from trusses and frameworks to three-dimensional solids. This is incorrect because the displacement under a concentrated load is infinite. He carefully regularizes the singular energy integral before stating the theorem.

Conclusions

The 1951 report provides concrete evidence that Fraeijs de Veubeke preceded both Hu and Washizu in the publication of the C4FLE functional. Furthermore, he appears to have been the first to construct a strain-displacement dual of the HR functional. Hence it seems fair to propose

1 that the canonical functional (12) be identified as the Fraeijs de Veubeke-Hu-Washizu functional.

2 that the hitherto anonymous strain displacement functional (13) be named after Fraeijs de Veubeke. This functional was constructed independently more than 20 years later by Oden and Reddy [10].

Some historical questions remain, perhaps as curiosities for future science historians.

Fraeijs de Veubeke was a visiting professor at MIT during 1952, the year following publication of the report examined here. Washizu's publication is an MIT report dated Mar. 1955. Professor Pian (private communication) has indicated to the writer that direct or indirect influence is unlikely, since Fraeijs de Veubeke was only a summer visitor.

The writer has not seen Washizu's 1955 report. However, in an early edition of his well-known monograph ([11]) the derivation of the C4FLE functional on pp. 31–34 closely follows Fraeijs de Veubeke's, as readers may verify. The similarity of Hu's and Washizu's paper titles is also puzzling.

Fraeijs de Veubeke does not reference Hu or Washizu in any of the papers reprinted in the Memorial Volume [12]. He acknowledges Friedrichs, Courant, Hilbert, Prager, Reissner, and Pian. On the other hand, he does not explicitly claim priority for the results discussed here. Perhaps he felt that the derivation of new functionals was not the focus of the 1951 report. And indeed it was not. The tour of five variational principles takes 8 pages out of 56. In contrast, the titles of the contributions of Hu and Washizu expressly state that to be the main objective. The writer's opinion is that Fraeijs de Veubeke's personality would militate against engaging in controversy. An aristocrat by birth and gentleman by nature, he never displayed greed for priority and recognition.

Acknowledgments

The writer is indebted to Profs. M. Geradin and P. Beckers of the University of Liège for locating and providing a copy of the 1951 report, and to Profs. T. H. H. Pian and J. N. Reddy for clarifying historical points.

References

[1] Hu, H.-C., 1955, ''On Some Variational Methods on the Theory of Elasticity and the Theory of Plasticity,'' Sci. Sin., **4**, pp. 33–54.

[2] Washizu, K., 1955, ''On the Variational Principles of Elasticity and Plasticity,'' Aeroelastic and Structures Research Laboratory, Technical Report 25-18, MIT, Cambridge, MA.

[3] Fraeijs de Veubeke, B. M., 1965, ''Displacement and Equilibrium Models,'' *Stress Analysis*, O. C. Zienkiewicz and G. Hollister, eds., Wiley, London, pp. 145–197.

[4] Fraeijs de Veubeke, B. M., 1951, ''Diffusion des Inconnues Hyperstatiques dans les Voilures à Longeron Couplés,'' *Bull. Serv. Technique de L'Aéronautique No. 24*, Imprimerie Marcel Hayez, Bruxelles, 56 pp.

[5] Fraeijs de Veubeke, B. M., 1974, ''Variational Principles and the Patch Test,'' Int. J. Numer. Methods Eng., **8**, pp. 783–801.

[6] Reissner, E., 1950, ''On a Variational Theorem in Elasticity,'' J. Math. Phys., **29**, pp. 90–95.

[7] Gurtin, M. E., 1983, ''The Linear Theory of Elasticity,'' *Mechanics of Solids Vol II*, C. Truesdell, ed., Springer-Verlag, Berlin, pp. 1–296.

[8] Felippa, C. A., 1994, ''A Survey of Parametrized Variational Principles and Applications to Computational Mechanics,'' Comput. Methods Appl. Mech. Eng., **113**, pp. 109–139.

[9] Oden, J. T., and Reddy, J. N., 1982, *Variational Methods in Theoretical Mechanics*, Springer-Verlag, Berlin.

[10] Oden, J. T., and Reddy, J. N., 1974, ''On Dual Complementary Variational Principles in Mathematical Physics,'' Int. J. Eng. Sci., **12**, pp. 1–29.

[11] Washizu, K., 1968, *Variational Methods in Elasticity and Plasticity*, Pergamon Press, New York.

[12] Geradin, M., ed., 1980, *B. M. Fraeijs de Veubeke Memorial Volume of Selected Papers*, Sitthoff & Noordhoff, Alphen aan den Rijn, The Netherlands.

Logarithmic Stress Singularities Resulting From Various Boundary Conditions in Angular Corners of Plates Under Bending

G. B. Sinclair

Department of Mechanical Engineering, Carnegie Mellon University, Pittsburgh, PA 15213-3890

This note considers the occurrence of pure logarithmic singularities in angular elastic plates under bending within the context of classical theory. By paralleling the development of requirements for logarithmic singularities for plates in extension, requirements

Contributed by the Applied Mechanics Division of THE AMERICAN SOCIETY OF MECHANICAL ENGINEERS for publication in the ASME JOURNAL OF APPLIED MECHANICS. Manuscript received by the ASME Applied Mechanics Division, May 18, 1999; final revision, Oct. 19, 1999. Associate Technical Editor: J. R. Barber.

for log singularities in bending are developed, both for homogeneous boundary conditions on plate edges and for inhomogeneous. Using these singularity requirements, some 50-odd configurations with log singularities are identified, the great majority being for inhomogeneous boundary conditions.
[S0021-8936(00)00501-8]

1 Introduction

Elastic stress singularities are not of the real world. However, their presence in a stress analysis can be a real fact. Then it is essential that their participation be recognized if reasonable use is to be made of the analysis in the vicinity of the singularity. The objective of this note is to assist in achieving such recognition.

In particular, we are concerned with identifying configurations which can have pure logarithmic singularities—that is, stress resultants and attendant stresses which behave like $O(\ln r)$ as $r \to 0$. These are the weakest singularities that occur in elasticity. As a result, they can be the most difficult to detect with numerical methods. Asymptotic identification is thus especially useful in avoiding having them pass undetected.

For angular elastic plates in bending treated within classical fourth-order theory, Williams [1] identifies possible power singularities for a variety of homogeneous boundary conditions on the plate edges. No logarithmic singularities are identified in [1]. Logarithmic singularities can be found elsewhere in the literature, but these occur in concert with the far stronger singularities that attend concentrated loads. Examples may be found in Nádai [2] Article 49, and Timoshenko and Woinowsky-Krieger [3] Article 75. Pure logarithmic singularities for plates in bending within classical theory would not appear to be identified in the literature. Here, therefore, we seek to identify such singularities, and to do so when either homogeneous or inhomogeneous boundary conditions apply on plate edges.

We begin, in Section 2, with a formal statement of the class of asymptotic problems of interest. Then, in Section 3, we outline the development of requirements for pure logarithmic singularities. We close, in Section 4, with a tabulation of all the configurations found to be able to have log singularities.

2 Formulation

The angular plate region of interest is shown in Fig. 1. To describe this plate, we use cylindrical polar coordinates (r,θ,z) with origin O at the vertex of its midplane and $\theta=0$ along one of its edges. The plate has indefinite extent in the r-direction, thickness $2h$ in the z-direction, and subtends an angle ϕ at its vertex.

The displacement of primary concern is that in the z-direction, w. This displacement has associated moment resultants M_r, M_0, M_{r0}, as shown acting in a positive sense on an element in the $r\theta$-plane in Fig. 2(*a*). It also has associated shear resultants Q_r, Q_θ, as shown acting in a positive sense on an element in Fig. 2(*b*). All of these field quantities are taken to be independent of z. Hence, we can confine our attention to the two-dimensional region $\Re$ where

$$\Re=\{(r,\theta)\,|\,0<r<\infty,\ 0<\theta<\phi\}.$$

With these preliminaries in place, we can formulate the class of problems for asymptotic analysis as next.

We seek the out-of-plane displacement w, together with its associated moment resultants $M_r, M_\theta, M_{r\theta}$ and shear resultants Q_r, Q_θ, as functions of r, θ throughout $\Re$ complying with the following requirements. The displacement is to satisfy the displacement equation of equilibrium in the absence of both body forces and loading on the plate faces at $z=\pm h$,

$$\nabla^4 w=0, \tag{1}$$

on $\Re$, where $\nabla^4=\nabla^2(\nabla^2)$, $\nabla^2=\partial^2/\partial r^2+r^{-1}\partial/\partial r+r^{-2}\partial^2/\partial\theta^2$. The displacement and resultants are to satisfy the resultant-displacement relations for a homogeneous and isotropic, linear elastic plate,

$$\begin{Bmatrix} M_r \\ M_\theta \end{Bmatrix} = -k\left[\begin{Bmatrix} \nu \\ 1 \end{Bmatrix}\frac{\nabla^2 w}{1-\nu}\begin{Bmatrix} + \\ - \end{Bmatrix}\frac{\partial^2 w}{\partial r^2}\right], \quad M_{r\theta}=k\frac{\partial}{\partial r}\left(\frac{1}{r}\frac{\partial w}{\partial\theta}\right), \tag{2}$$

$$Q_r=\frac{-k}{1-\nu}\frac{\partial}{\partial r}(\nabla^2 w), \quad Q_\theta=\frac{-k}{1-\nu}\frac{1}{r}\frac{\partial}{\partial\theta}(\nabla^2 w),$$

on $\Re$, where $k=4\mu h^3/3$ is the flexural stiffness of the plate while μ, ν are its shear modulus, Poisson's ratio. The displacement/resultants are to satisfy any one of the admissible sets of boundary conditions listed in Table 1 on the plate edge at $\theta=0$, as well as a further such set on $\theta=\phi$. Finally, the resultants are to comply with the following regularity-singularity requirement:

$$M=O(1), \quad Q=O(\ln r), \ \text{as} \ r\to 0, \tag{3}$$

on $\Re$, where M is any moment resultant, Q either shear resultant.

Several comments on the foregoing formulation are in order. First, regarding the boundary conditions in Table 1. In conditions I–III, M_i, V, a_i, and b are given constants $(i=1,2)$. When these constants are zero, we obtain the corresponding homogeneous boundary conditions. We distinguish these with a subscript h. Thus I_h are Kirchhoff conditions for a stress-free edge, II_h are for a simply supported edge, and III_h are for a built-in edge. Conditions IV model a plate edge which is elastically restrained by a bar: k_t is the bar's torsional stiffness, k_b its bending stiffness, and plus signs are for $\theta=\phi$, minus for $\theta=0$.[1]

Second, regarding the regularity-singularity requirement. For the usual relationships between stress resultants and stresses in plate theory, this has pure log singularities in $\tau_{rz}, \tau_{\theta z}$ while $\sigma_r, \sigma_\theta, \tau_{r\theta}$ are nonsingular.

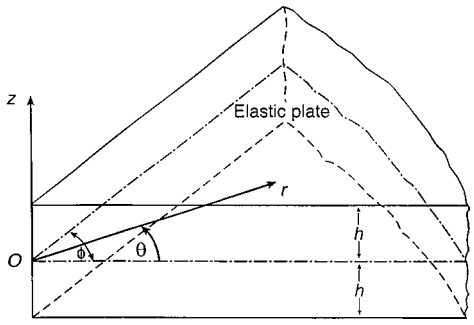

Fig. 1 Geometry and coordinates for the angular elastic plate

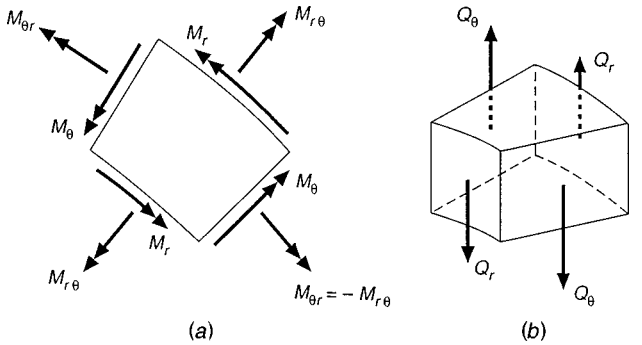

Fig. 2 Plate theory resultants: (*a*) moment resultants, (*b*) shear resultants

[1] See [3], Art. 22, for a development of IV.

Table 1 Boundary conditions

Assigned Roman Numeral	Physical Description	Prescribed Quantities
I	Applied moment/shear	$M_\theta = M_1 r$
	$Q_\theta - \frac{\partial m_{r\theta}}{\partial r}$	$Q_\theta - \frac{\partial M_{r\theta}}{\partial r} = V$
II	Applied moment/displacement	$M_\theta = M_2 r$
		$w = a_1 r^3$
III	Applied displacement/rotation	$w = a_2 r^3$
		$\frac{\partial w}{\partial \theta} = b r^3$
IV	Elastically restrained	$M_\theta = \pm k_t \frac{\partial^2}{\partial r^2}\left(\frac{1}{r}\frac{\partial w}{\partial \theta}\right)$
		$Q_\theta - \frac{\partial M_{r\theta}}{\partial r} \pm k_b \frac{\partial^4 w}{\partial r^4} = 0$

Table 2 Eigenvalue equations

Boundary Conditions on $\theta = 0, \phi$	Eigenvalue Equation
I_h–I_h	$(\lambda-1)^2(\kappa^2 \sin^2 \lambda\phi - \lambda^2 \sin^2 \phi) = 0$
II_h–II_h	$\cos^2 \lambda\phi - \cos^2 \phi = 0$
III_h or IV–III_h or IV	$\sin^2 \lambda\phi - \lambda^2 \sin^2 \phi = 0$
I_h–II_h	$(\lambda-1)(\kappa \sin 2\lambda\phi + \lambda \sin 2\phi) = 0$
I_h–III_h or IV	$(\lambda-1)(\kappa^2 + 2\kappa \cos 2\lambda\phi + 1 - 4\lambda^2 \sin^2 \phi) = 0$
II_h–III_h or IV	$\sin 2\lambda\phi - \lambda \sin 2\phi = 0$

3 Analysis

As in the extensional case, requirements for logarithmic singularities under bending follow from a further development of the corresponding classical analysis for power singularities. Accordingly we next summarize the asymptotic analysis of power singularities in plates under bending.

In Williams [1], the appropriate choice of a separable biharmonic function for the displacement w leads to fields containing four constants which share a common power of r. This function has the form

$$w = r^{\lambda+1}[c_1 \sin(\lambda+1)\theta + c_2 \cos(\lambda+1)\theta + c_3 \sin(\lambda-1)\theta + c_4 \cos(\lambda-1)\theta], \quad (4)$$

where c_j $(j = 1-4)$ are the four constants, and λ is the separation-of-variables parameter. The stress resultants for this basic field follow from (2). Substituting these fields into a set of four homogeneous boundary conditions then gives

$$\mathbf{Ac} = \mathbf{0}, \quad (5)$$

where the vector $\mathbf{c} = (c_1, c_2, c_3, c_4)$, and $\mathbf{A}$ is a matrix whose elements are in general functions of λ. A nontrivial solution to (5) requires that the determinant D of $\mathbf{A}$ satisfy

$$D = 0. \quad (6)$$

This requirement generates an eigenvalue equation for λ. Determining λ satisfying (6) with $0 < \mathrm{Re}\,\lambda < 2$ then characterizes the power singularities possible in stress resultants for the particular homogeneous boundary conditions involved.

To extend the preceding to consider logarithmic singularities, we need stress resultants containing $\ln r$ terms. To this end, we differentiate the basic field of (4) with respect to λ: thus

Table 3 Configurations with $Q = O(1nr)$ as $r \to 0$

Boundary Conditions on $\theta = 0, \phi$	Configuration Specifications
I–I_h	$\phi = \pi$ or 2π, $M_1 \neq 0$ or $V \neq 0$
	$\kappa = \pm\sec\phi$, $M_1(\kappa+2)\left(\tan\frac{\phi}{2}\right)^{\pm 1} \neq \pm V(2-\kappa)$,
II–II_h	$\phi = \pi$ or 2π, $M_2 \neq 6a_1 k$
III–III_h or IV	$\phi = \pi$ or 2π, $a_2 \neq 0$ or $b \neq 0$
I–II	$\phi = (2m-1)\frac{\pi}{2}$, $24a_1 k \neq M_2(\kappa+5) - (-)^m V(\kappa+1)$ $(m = 1,2)$
	$\phi = m\pi$, $M_1 \neq (-)^m M_2$ $(m = 1,2)$
	$\kappa = -\sec 2\phi$, $(V \sin\phi - 12a_1 k)(\kappa-2) \neq M_1(\kappa+2)\cos\phi - M_2(\kappa-4)$
I–III	$\phi = \phi_\kappa$, $\kappa \neq \hat{\kappa}$, $(M_1 - 6a_2 k \cos 3\phi)(3\sin 3\phi - (\kappa+2)\sin\phi)$ $\neq (V + 2bk \cos 3\phi)(3\cos 3\phi + (\kappa-2)\cos\phi)$
I_h–III_h or IV	$\phi = \hat{\phi}_\kappa$, $\kappa = \hat{\kappa}$
I–IV	$\phi = \pi$ or 2π, $V \neq 0$
	$\phi = \pi/2$ or $3\pi/2$, $M_1 \neq 0$
	$\kappa = -\sec 2\phi$, $M_1(\kappa+2)\tan\phi \neq V(2-\kappa)$
II–III	$\phi = (2m-1)\frac{\pi}{2}$, $2M_2 \neq 3(3-\kappa)a_1 k - (-)^m(\kappa+1)bk$ $(m = 1,2)$
	$\phi = m\pi$, $a_1 \neq (-)^m a_2$ $(m = 1,2)$
II–IV	$\phi = \pi/2$ or $3\pi/2$, $M_2 \neq 6a_1 k$
III–IV	$\phi = \pi/2$ or $3\pi/2$, $a_2 \neq 0$
	$\phi = \pi$ or 2π, $b \neq 0$

$$w = r^{\lambda+1}[\ln r(\bar{c}\sin(\lambda+1)\theta + \bar{c}_2\cos(\lambda+1)\theta + \bar{c}_3\sin(\lambda-1)\theta + \bar{c}_4\cos(\lambda-1)\theta) + \theta(\bar{c}_1\cos(\lambda+1)\theta - \bar{c}_2\sin(\lambda+1)\theta + \bar{c}_3\cos(\lambda-1)\theta - \bar{c}_4\sin(\lambda-1)\theta)], \quad (7)$$

where the bars atop constants serve to indicate that they no longer need be the same as their antecedents in (4). The displacement in (7) continues to satisfy the governing biharmonic Eq. (1). Substituting (7) into (2) produces resultants containing $\ln r$ terms. Substituting (7) and these last, together with the original basic fields, into a set of four homogeneous boundary conditions gives

$$\mathbf{A}\bar{\mathbf{c}}\ln\mathbf{r} + \frac{d\mathbf{A}}{d\lambda}\bar{\mathbf{c}} + \mathbf{A}\mathbf{c} = \mathbf{0}, \quad (8)$$

where $d\mathbf{A}/d\lambda$ is formed from $\mathbf{A}$ by differentiating each element with respect to λ. General requirements for a nontrivial solution for $\bar{\mathbf{c}}$ in (8) are established in Dempsey and Sinclair [4]. From these we obtain our *requirements for pure logarithmic singularities under homogeneous boundary conditions*:

$$\lambda = 2, \quad D = 0, \quad (9a)$$

$$\frac{d^n D}{d\lambda^n} = 0 \quad \text{for} \quad n = 1, \ldots, 4 - r_A, \quad (9b)$$

$$\bar{c}_3^2 + \bar{c}_4^2 \neq 0, \quad (9c)$$

where r_A is the rank of $\mathbf{A}$ when $\lambda = 2$. Equation (9*c*) ensures that one of $\bar{c}_3$ or $\bar{c}_4$ is not zero so that the shear resultants are indeed logarithmically singular as in (3).

Turning to the inhomogeneous boundary conditions I–III of Table 1, we obtain instead of (5)

$$\mathbf{A}\mathbf{c} = \mathbf{f}, \quad (10)$$

for $\lambda = 2$, where $\mathbf{f}$ is a vector whose components involve one or more of M_i, V, a_i, and b $(i = 1,2)$. For $\mathbf{f} \neq \mathbf{0}$, we have a problem in (10) if $D = 0$ for $\lambda = 2$, unless the rank of the augmented matrix, $(\mathbf{A}') = (\mathbf{A}:\mathbf{f})$, is also reduced. If this rank reduction does not occur, we can overcome the difficulty by again supplementing the basic fields associated with (4) with the auxiliary ones stemming from (7).[2] This gives

$$\mathbf{A}\bar{\mathbf{c}}\ln\mathbf{r} + \frac{d\mathbf{A}}{d\lambda}\bar{c} + \mathbf{A}\mathbf{c} = \mathbf{f}, \quad (11)$$

for $\lambda = 2$. The system in (11) can be solved provided all the requirements in (9*b*) are *not* met. Accordingly our *requirements for pure logarithmic singularities under inhomogeneous boundary conditions* are

$$\lambda = 2, \quad D = 0, \quad r_A' \neq r_A, \quad (12a)$$

$$\frac{d^n D}{d\lambda^n} \neq 0 \quad \text{for at least one} \quad n = 1, \ldots, 4 - r_A, \quad (12b)$$

$$\bar{c}_3^2 + \bar{c}_4^2 \neq 0, \quad (12c)$$

where r_A' is the rank of $\mathbf{A}'$ when $\lambda = 2$. As with (9*c*), (12*c*) ensures (3) is complied with when $\lambda = 2$.

An additional set of requirements for logarithmic singularities under inhomogeneous boundary conditions is given in Sinclair [7] for the extensional case. These requirements arise from further auxiliary fields which result from a further differentiation with respect to λ. However, we omit these requirements here because they can never be completely satisfied for the class of problems treated. Subsequently we do note, though, the one instance of a log-squared singularity that attends partial compliance with them.

With the requirements for logarithmic singularities at hand, analysis proceeds routinely. We first derive eigenvalue equations as in (6) for all possible combinations of homogeneous boundary conditions that can be drawn from Table 1. Then we check (9) and (12). When potential new configurations with log singularities are revealed, the last requirement in either (9) or (12) requires the assembling of associated new fields. The algebra involved is straightforward but lengthy: details are furnished in Sinclair [8]. Displacements with log singularities in their companion resultants are set out ibid. All of these fields are verified directly by substituting them into the governing Eqs. (1),(2), checking the regularity-singularity requirement (3), and checking the pertinent boundary conditions. In the interests of brevity, we omit these fields here and simply provide the configurations that engender them.

4 Results

Eigenvalue equations are set out in Table 2. Therein

$$\kappa = \frac{3+\nu}{1-\nu}.$$

Except for a factor of $(\lambda-1)$ when free-edge conditions, I_h, are involved, these equations are equivalent to those derived in Williams [1]. The equivalence of built-in conditions III_h with elastically restrained conditions IV, as far as eigenvalue equations are concerned, follows from an adaptation of the argument in Sinclair [9] for boundary conditions which have terms with a different r-dependence within a single condition. This equivalence holds for any value of λ. Just for $\lambda = 2$, elastically restrained conditions are equivalent to symmetry conditions, $\partial w/\partial\theta = 0$ and $Q_\theta = 0$. We also investigate them in this role in what follows.

Configurations which have logarithmic singularities in their shear resultants as in (3) are listed in Table 3. In Table 3, ϕ_κ is such that

$$\sin^2\phi_\kappa = \frac{\kappa+1}{4\kappa}[2 \pm \sqrt{4-\kappa}]. \quad (13)$$

If in addition to (13),

$$\kappa = \frac{-\tan\phi}{\phi\cos 2\phi},$$

then $\kappa = \hat{\kappa}$, $\phi_\kappa = \hat{\phi}_\kappa$ (actual values in the physical range of $3 \leqslant \kappa \leqslant 7$ are $\hat{\kappa} = 3.27$, $\hat{\phi}_\kappa = 74.8$ deg and $\hat{\kappa} = 3.02$, $\hat{\phi}_\kappa = 265.9$ deg.). For I–II and $\phi = \hat{\phi}_\kappa$, $\kappa = \hat{\kappa}$, a log-squared singularity occurs.

There are but two geometries with logarithmic singularities under completely homogeneous conditions in Table 3. These occur for $\kappa = \hat{\kappa}$, $\phi = \hat{\phi}_\kappa$ when the boundary conditions are $\mathrm{I}_h - \mathrm{III}_h$ or IV. One of these geometries is a re-entrant corner ($\hat{\phi}_\kappa = 265.9$ deg) and so is not surprising, but the other is for a proud corner ($\hat{\phi}_\kappa = 74.8$ deg). Here, then, the increase in the occurrence of singularities with mixed boundary conditions is making its presence felt, as it does in the extensional case.

For inhomogeneous boundary conditions, there are a number of quite innocent looking configurations with log singularities in Table 3. For example, $\mathrm{I}-\mathrm{I}_h$ for $\phi = \pi$ when $M_\theta = M_1 r$: Here the moment resultant actually varies continuously along the boundary, though its derivative does not.

References

[1] Williams, M. L., 1951, ''Surface Stress Singularities Resulting From Various Boundary Conditions in Angular Corners of Plates Under Bending,'' *Proceedings of the First U.S. National Congress of Applied Mechanics*, Illinois Institute of Technology, Chicago, pp. 325–329.

[2] Nádai, A., 1925, *Die elastischen Platten*, Julius Springer Publishing, Berlin.

[3] Timoshenko, S. P., and Woinowsky-Krieger, S., 1959, *Theory of Plates and Shells*, 2nd Ed. McGraw-Hill, New York.

[2] Essentially this is the approach adopted in Dimpsey [5] to solve extensional Levy problems for certain critical wedge angles. An alternative approach for these problems is furnished in Ting [6]. The latter yields the same logarithmic fields for the critical angles, and has the added attribute of effecting a sensible evolution of stresses as the critical angles are passed through. It could be adapted to the class of problems of concern here if one sought a corresponding evolution of responses.

[4] Dempsey, J. P., and Sinclair, G. B., 1979, ''On the Stress Singularities in the Plane Elasticity of the Composite Wedge,'' J. Elast., **9**, pp. 373–391.
[5] Dempsey, J. P., 1981, ''The Wedge Subjected to Tractions: A Paradox Resolved,'' J. Elast., **11**, pp. 1–10.
[6] Ting, T. C. T., 1984, ''The Wedge Subjected to Tractions: A Paradox Re-Examined,'' J. Elast., **14**, pp. 235–247.
[7] Sinclair, G. B., 1999, ''Logarithmic Stress Singularities Resulting From Various Boundary Conditions in Angular Corners of Plates in Extension,'' ASME J. Appl. Mech., **66**, pp. 556–560.
[8] Sinclair, G. B., 1999, ''Analysis of Logarithmic Stress Singularities Resulting from Various Boundary Conditions in Angular Elastic Plates in Bending,'' Report SM 99-1, Department of Mechanical Engineering, Carnegie Mellon University, Pittsburgh, PA.
[9] Sinclair, G. B., 1980, ''On the Singular Eigenfunctions for Plane Harmonic Problems in Composite Regions,'' ASME J. Appl. Mech., **47**, pp. 87–92.

Stress and Displacement Fields for Propagating the Crack Along the Interface of Dissimilar Orthotropic Materials Under Dynamic Mode I and II Load

K. H. Lee
Department of Automotive Engineering, Sangju National University, Sangju City, Kyungbuk 742-711, Korea

General stress and displacement fields are derived as a crack steadily propagates along the interface of dissimilar orthotropic materials under a dynamic mode I and II load. They are obtained from the complex function formulation of steady plane motion problems for an orthotropic material and the complex eigenexpansion function. After the relationship between stress intensity factors and stress components for a propagating crack is defined, the stress, displacement components, and energy release rate with stress intensity factors are derived. The results are useful for both dissimilar isotropic and orthotropic and isotropic-orthotropic bimaterials, and homogeneous isotropic and orthotropic materials under subsonic crack propagation velocity.
[S0021-8936(00)00601-2]

1 Introduction

Yang et al. [1] and Deng [2] provided the asymptotic fields of the singular terms of steady-state elastodynamic bimaterial crack-tip fields and Liu et al. [3] obtained the asymptotic series representation of stress fields near the tip of a running interfacial crack in a bimaterial under steady or unsteady state conditions. However, the stress and displacement components for the interfacial propagating crack in dissimilar orthotropic media, where the elastic principal axis direction with the crack direction is orthogonal or parallel, is not clearly represented.

Therefore, the general stress and displacement fields are derived when a finite crack is steadily propagated along the interface in dissimilar orthotropic media under dynamic mode I and II loading in the paper. Lee et al. [4] derived the steady plane motion formulations for orthotropic material from the partial differential equation for an elastodynamic plane. The general stress and displacement fields are obtained from the formulation of steady plane motion which is added to the complex eigenexpansion functions and the boundary conditions. The relationship between stress intensity factors and stress components for propagating an interfacial crack is defined and the confusion of the definition for the stress intensity factors of the interface crack is clarified.

Contributed by the Applied Mechanics Division of THE AMERICAN SOCIETY OF MECHANICAL ENGINEERS for publication in the ASME JOURNAL OF APPLIED MECHANICS. Manuscript received by the ASME Applied Mechanics Division, June 23, 1999; final revision, Oct. 12, 1999. Associate Technical Editor: W. J. Drugan.

2 General Stress and Displacement Fields

When characteristic roots m_l and m_s of orthotropic material have imaginary numbers ip, iq, the complex stress for orthotropic plane motion can be represented as Eq. (1) [4],

$$\sigma_x = 2\,\mathrm{Re}\{(M_b - p^2)\phi'(z_l) + (M_b - q^2)\psi'(z_s)\}$$
$$\sigma_y = 2\,\mathrm{Re}\{(1+M_a)[\phi'(z_l) + \psi'(z_s)]\} \tag{1}$$
$$\tau_{xy} = 2\,\mathrm{Im}[\alpha_l\phi'(z_l) + \alpha_s\psi'(z_s)]\}$$

where

$$p = \sqrt{B_{12} - \sqrt{B_{12}^2 - K_{66}}}, \quad q = \sqrt{B_{12} + \sqrt{B_{12}^2 - K_{66}}}$$

$$B_{12} = \frac{1}{2}[2a_{12} + a_{66} + \rho c^2(a_{12}^2 - a_{11}a_{66} - a_{11}a_{22})]/a_{11}$$

$$K_{66} = \{a_{22} + \rho c^2[a_{12}^2 - a_{22}a_{66} - a_{11}a_{22} + \rho c^2 a_{66}(a_{11}a_{22} - a_{12}^2)]\}/a_{11}$$

$$\alpha_l = p + a_{22}\frac{\rho c^2}{p} - p\rho c^2 a_{11} - \frac{(\rho c^2)^2}{p}(a_{11}a_{22} - a_{12}^2)$$

$$\alpha_s = q + a_{22}\frac{\rho c^2}{q} - q\rho c^2 a_{11} - \frac{(\rho c^2)^2}{q}(a_{11}a_{22} - a_{12}^2)$$

$$M_a = \rho c^2(a_{12} - a_{11}), \quad M_b = \rho c^2(a_{12} - a_{22}).$$

$a_{ij}(i,j = 1,2,3,\ldots,6)$ are displacement constants, which are the $a_{i3} = a_{j3} = 0$ for plane stress and are transformed into the $b_{ij} = a_{ij} - a_{i3}a_{j3}/a_{33}$ for plane strain [5]. The ρ and c are, respectively, density and crack propagation velocity. And the characteristic roots m_l, m_s of orthotropic materials, which depend on the physical properties and the crack propagation, are either imaginary when $\sqrt{K_{66}} < B_{12}$; $K_{66} > 0$ or complex when $\sqrt{K_{66}} > |B_{12}|$; $K_{66} > 0$ [4]. Most orthotropic materials have imaginary number roots. The complex displacement for orthotropic plane motion can be represented as Eq. (2) [4],

$$u_x = 2\,\mathrm{Re}[p_l\phi(z_l) + p_s\psi(z_s)]$$
$$u_y = 2\,\mathrm{Im}[q_l\phi(z_l) + q_s\psi(z_s)] \tag{2}$$

where

$$p_l = a_{11}(M_b - p^2) + a_{12}(M_a + 1)$$

$$p_s = a_{11}(M_b - q^2) + a_{12}(M_a + 1)$$

$$q_l = [a_{12}(M_b - p^2) + a_{22}(M_a + 1)]/p$$

$$q_s = [a_{12}(M_b - q^2) + a_{22}(M_a + 1)]/q.$$

Analytical complex functions $\phi'(z_l)$ and $\psi'(z_s)$ can be represented as such a power series in

$$\phi'(z_l) = az_l^{\lambda_n} + b\overline{z_l^{\lambda_n}}, \quad \psi'(z_s) = cz_s^{\lambda n} + d\overline{z_s^{\lambda_n}} \tag{3}$$

where a, b, c, and d are complex constants and λ_n is an eigenvalue. They are to be determined from boundary conditions. From the traction-free crack ($\theta=\pm\pi$) and the traction and displacement continuous condition across interface ($\theta=0$), the following equations can be obtained:

$$e^{i2\pi\lambda_n}[S]_1\begin{bmatrix}a_1\\c_1\end{bmatrix}=[T]_1\overline{\begin{bmatrix}b_1\\d_1\end{bmatrix}} \tag{4}$$

$$e^{-i2\pi\lambda_n}[S]_2\begin{bmatrix}a_2\\c_2\end{bmatrix}=[T]_2\overline{\begin{bmatrix}b_2\\d_2\end{bmatrix}} \tag{5}$$

$$[S]_1\begin{bmatrix}a_1\\c_1\end{bmatrix}-[T]_1\overline{\begin{bmatrix}b_1\\d_1\end{bmatrix}}=[S]_2\begin{bmatrix}a_2\\c_2\end{bmatrix}-[T]_2\overline{\begin{bmatrix}b_2\\d_2\end{bmatrix}} \tag{6}$$

$$[U]_1\begin{bmatrix}a_1\\c_1\end{bmatrix}-[V]_1\overline{\begin{bmatrix}b_1\\d_1\end{bmatrix}}=[U]_2\begin{bmatrix}a_2\\c_2\end{bmatrix}-[V]_2\overline{\begin{bmatrix}b_2\\d_2\end{bmatrix}} \tag{7}$$

where

$$S_k=\begin{bmatrix}(1+M_a) & (1+M_a)\\ \alpha_l & \alpha_s\end{bmatrix},\quad T_k=\begin{bmatrix}-(1+M_a) & -(1+M_a)\\ \alpha_l & \alpha_s\end{bmatrix}$$

$$U_k=\begin{bmatrix}-p_l & -p_s\\ q_l & q_s\end{bmatrix},\quad V_k=\begin{bmatrix}p_l & p_s\\ q_l & q_s\end{bmatrix}.$$

Matrices L_k, L_k^*, H_k, and H_k^* input as follows:

$$L_k=U_kS_k^{-1},\quad L_k^*=V_kT_k^{-1}$$
$$H=L_1-L_2^*,\quad H^*=L_1^*-L_2. \tag{8}$$

Substituting Eq. (8) into Eqs. (4)–(7), the characteristic equation can be derived for eigenvalue λ_n,

$$\begin{bmatrix}\lambda_2 & 0\\ 0 & \lambda_1\end{bmatrix}(e^{i2\pi\lambda_n})^2-\begin{bmatrix}\lambda_1+\lambda_2 & 0\\ 0 & \lambda_1+\lambda_2\end{bmatrix}(e^{i2\pi\lambda_n})+\begin{bmatrix}\lambda_1 & 0\\ 0 & \lambda_2\end{bmatrix}=0 \tag{9}$$

where

$$\lambda_1=h_{11}+\sqrt{h_{12}h_{21}},\quad \lambda_2=h_{11}-\sqrt{h_{12}h_{21}}$$

$$h_{11}=(l_{11})_1-(l_{11})_2,\quad h_{12}=(l_{12})_1+(l_{12})_2$$

$$h_{21}=(l_{21})_1+(l_{21})_2$$

$$(l_{11})_k=\left\{\frac{p_s\alpha_l-p_l\alpha_s}{D}\right\}_k=\left\{\frac{q_s-q_l}{\alpha_s-\alpha_l}\right\}_k$$

$$(l_{12})_k=\left\{\frac{(1+M_\alpha)(p_l-p_s)}{D}\right\}_k,\quad (l_{21})_k=\left\{\frac{\alpha_sq_l-\alpha_lq_s}{D}\right\}_k$$

$$D_k=[(1+M_a)(\alpha_s-\alpha_l)]_k.$$

When $D_k=0$, the crack propagation velocity c becomes the Rayleigh speed. From Eq. (9), eigenvalue λ_n can be determined as Eq. (10).

$$\lambda_n=\begin{cases}n\ \ (=0,1,2,3,\dots)\\ \dfrac{2n-1}{2}\pm i\varepsilon\ \ (n=0,1,2,3,\dots)\end{cases} \tag{10}$$

$$\varepsilon=\frac{1}{2\pi}\ln\frac{1-\beta}{1+\beta},\quad \beta=\frac{h_{11}}{\sqrt{h_{12}h_{21}}}$$

Therefore the two cases, oscillatory and nonoscillatory fields, must be considered.

2.1 Oscillatory Stress and Displacement Fields. The λ_n is a complex eigenvalue in this case. Therefore, in substituting the complex eigenvalue $\lambda_n=(2n-1)/2+i\varepsilon$ in Eq. (10) into Eqs. (4)–(7), complex constants a_k, b_k, c_k, and d_k may be obtained as

$$a_k=\left[\frac{\alpha_s-(1+M_a)\eta}{D}\right]_k e^{\pi\varepsilon(-1)^{k+1}}\zeta$$

$$b_k=\left[\frac{\alpha_s+(1+M_a)\eta}{D}\right]_k e^{\pi\varepsilon(-1)^{k}}\overline{\zeta}$$

$$c_k=\left[\frac{-\alpha_l+(1+M_a)\eta}{D}\right]_k e^{\pi\varepsilon(-1)^{k+1}}\zeta$$

$$d_k=-\left[\frac{\alpha_l+(1+M_a)\eta}{D}\right]_k e^{\pi\varepsilon(-1)^{k}}\overline{\zeta} \tag{11}$$

where $\eta=(h_{21}/h_{12})^{1/2}$ and ζ is a complex constant related to stress intensity factors. Substituting Eq. (11) into Eq. (3), $\phi'_{n1}(z_l)$ and $\psi'_{n1}(z_s)$ for material 1 are written as

$$\phi'_{n1}(z_l)=\frac{z_l^{(2n-1)/2}}{D_1}\{[\alpha_s-(1+M_a)\eta]e^{\varepsilon\pi}\zeta_nz_l^{i\varepsilon}+[\alpha_s+(1+M_a)\eta]e^{-\varepsilon\pi}\overline{\zeta_nz_s^{-i\varepsilon}}\}$$

$$\psi'_{n1}(z_s)=\frac{z_s^{(2n-1)/2}}{D_1}\{[-\alpha_l+(1+M_a)\eta]e^{\varepsilon\pi}\zeta_nz_l^{i\varepsilon}-[\alpha_s+(1+M_a)\eta]e^{-\varepsilon\pi}\overline{\zeta_nz_s^{-i\varepsilon}}\}. \tag{12}$$

Stress intensity factors can be defined as Eq. (13) when the crack is propagated along the interface in dissimilar media.

$$K_{\mathrm{I}}+iK_{\mathrm{II}}=\lim_{r\to0}\sqrt{2\pi r}r^{-i\varepsilon}\left(\sigma_y+i\frac{1}{\eta}\tau_{xy}\right)_{\theta=0}. \tag{13}$$

In substituting Eq. (12) into Eq. (1) and substituting Eq. (1) into Eq. (13), the complex constants related to stress intensity factors are obtained as Eq. (14),

$$K_n^0=2\sqrt{2\pi}(e^{\varepsilon\pi}+e^{-\varepsilon\pi})\zeta_n^0$$
$$K_n^*=2\sqrt{2\pi}(e^{\varepsilon\pi}+e^{-\varepsilon\pi})\zeta_n^*, \tag{14}$$

where ζ_n^0 and ζ_n^* are real parts of complex constant ζ_n. When $n=0$ in Eq. (14), K_n^0 and K_n^* are stress intensity factors K_{I} and K_{II}. In substituting Eq. (14) into Eq. (12) and substituting Eq. (12) into Eq. (1), stress fields for propagating the crack along the interface in dissimilar orthotropic material can be obtained. Oscillatory stress fields with odd power series ($n=1,3,5,\dots$) for material 1 (the material above the interface) can be represented as

$$\sigma_{xn}=\sum_{n=\text{odd}}^{\infty}\frac{K_n^0}{2\sqrt{2\pi}D\,\cosh(\varepsilon\pi)}\Bigg[(M_b-p^2)\Bigg\{e^{\varepsilon(\pi-\theta_l)}\overline{A}\,\cos\Big(\varepsilon\,\ln r_l+\frac{n-2}{2}\theta_l\Big)+e^{-\varepsilon(\pi-\theta_l)}A\,\cos\Big(\varepsilon\,\ln r_l-\frac{n-2}{2}\theta_1\Big)\Bigg\}r_l^{(n-2)/2}$$
$$-(M_b-q^2)\Bigg\{e^{\varepsilon(\pi-\theta_s)}\overline{B}\,\cos\Big(\varepsilon\,\ln r_s+\frac{n-2}{2}\theta_s\Big)+e^{-\varepsilon(\pi-\theta_s)}B\,\cos\Big(\varepsilon\,\ln r_s-\frac{n-2}{2}\theta_s\Big)\Bigg\}r_s^{(n-2)/2}\Bigg]$$
$$+\sum_{n=\text{odd}}^{\infty}\frac{K_n^*}{2\sqrt{2\pi}D\,\cosh(\varepsilon\pi)}\Bigg[-(M_b-p^2)\Bigg\{e^{\varepsilon(\pi-\theta_l)}\overline{A}\,\sin\Big(\varepsilon\,\ln r_l+\frac{n-2}{2}\theta_l\Big)+e^{-\varepsilon(\pi-\theta_l)}A\,\sin\Big(\varepsilon\,\ln r_l-\frac{n-2}{2}\theta_l\Big)\Bigg\}r_l^{(n-2)/2}$$
$$+(M_b-q^2)\Bigg\{e^{\varepsilon(\pi-\theta_s)}\overline{B}\,\sin\Big(\varepsilon\,\ln r_s+\frac{n-2}{2}\theta_s\Big)+e^{-\varepsilon(\pi-\theta_s)}B\,\sin\Big(\varepsilon\,\ln r_s-\frac{n-2}{2}\theta_s\Big)\Bigg\}r_s^{(n-2)/2}\Bigg] \tag{15}$$

$$\sigma_{yn}=\sum_{n=\text{odd}}^{\infty}\frac{K_n^0}{2\sqrt{2\pi}D\,\cosh(\varepsilon\pi)}\Bigg[(1+M_a)\Bigg\{e^{\varepsilon(\pi-\theta_l)}\overline{A}\,\cos\Big(\varepsilon\,\ln r_l+\frac{n-2}{2}\theta_l\Big)+e^{-\varepsilon(\pi-\theta_l)}A\,\cos\Big(\varepsilon\,\ln r_l-\frac{n-2}{2}\theta_l\Big)\Bigg\}r_l^{(n-2)/2}$$
$$-(1+M_a)\Bigg\{e^{\varepsilon(\pi-\theta_s)}\overline{B}\,\cos\Big(\varepsilon\,\ln r_s+\frac{n-2}{2}\theta_s\Big)+e^{-\varepsilon(\pi-\theta_s)}B\,\cos\Big(\varepsilon\,\ln r_s-\frac{n-2}{2}\theta_s\Big)\Bigg\}r_s^{(n-2)/2}\Bigg]$$
$$+\sum_{n=\text{odd}}^{\infty}\frac{K_n^*}{2\sqrt{2\pi}D\,\cosh(\varepsilon\pi)}\Bigg[-(1+M_a)\Bigg\{e^{\varepsilon(\pi-\theta_l)}\overline{A}\,\sin\Big(\varepsilon\,\ln r_l+\frac{n-2}{2}\theta_l\Big)+e^{-\varepsilon(\pi-\theta_l)}A\,\sin\Big(\varepsilon\,\ln r_l-\frac{n-2}{2}\theta_l\Big)\Bigg\}r_l^{(n-2)/2}$$
$$+(1+M_a)\Bigg\{e^{\varepsilon(\pi-\theta_s)}\overline{B}\,\sin\Big(\varepsilon\,\ln r_s+\frac{n-2}{2}\theta_s\Big)+e^{-\varepsilon(\pi-\theta_s)}B\,\sin\Big(\varepsilon\,\ln r_s-\frac{n-2}{2}\theta_s\Big)\Bigg\}r_s^{(n-2)/2}\Bigg] \tag{16}$$

$$\tau_{xyn}=\sum_{n=\text{odd}}^{\infty}\frac{K_n^0}{2\sqrt{2\pi}D\,\cosh(\varepsilon\pi)}\Bigg[\alpha_l\Bigg\{e^{\varepsilon(\pi-\theta_l)}\overline{A}\,\sin\Big(\varepsilon\,\ln r_l+\frac{n-2}{2}\theta_l\Big)-e^{-\varepsilon(\pi-\theta_l)}A\,\sin\Big(\varepsilon\,\ln r_l-\frac{n-2}{2}\theta_l\Big)\Bigg\}r_l^{(n-2)/2}$$
$$+\alpha_s\Bigg\{-e^{\varepsilon(\pi-\theta_s)}\overline{B}\,\sin\Big(\varepsilon\,\ln r_s+\frac{n-2}{2}\theta_s\Big)+e^{-\varepsilon(\pi-\theta_s)}B\,\sin\Big(\varepsilon\,\ln r_s-\frac{n-2}{2}\theta_s\Big)\Bigg\}r_s^{(n-2)/2}\Bigg]$$
$$+\sum_{n=\text{odd}}^{\infty}\frac{K_n^*}{2\sqrt{2\pi}D\,\cosh(\varepsilon\pi)}\Bigg[\alpha_l\Bigg\{e^{\varepsilon(\pi-\theta_l)}\overline{A}\,\cos\Big(\varepsilon\,\ln r_l+\frac{n-2}{2}\theta_l\Big)-e^{-\varepsilon(\pi-\theta_l)}A\,\cos\Big(\varepsilon\,\ln r_l-\frac{n-2}{2}\theta_l\Big)\Bigg\}r_l^{(n-2)/2}$$
$$+\alpha_s\Bigg\{-e^{\varepsilon(\pi-\theta_s)}\overline{B}\,\cos\Big(\varepsilon\,\ln r_s+\frac{n-2}{2}\theta_s\Big)+e^{-\varepsilon(\pi-\theta_s)}B\,\cos\Big(\varepsilon\,\ln r_s-\frac{n-2}{2}\theta_s\Big)\Bigg\}r_s^{(n-2)/2}\Bigg] \tag{17}$$

where

$$A=\alpha_s+(1+M_a)\,\eta,\quad \overline{A}=\alpha_s-(1+M_a)\,\eta,\quad B=\alpha_l+(1+M_a)\,\eta,\quad \overline{B}=\alpha_l-(1+M_a)\,\eta.$$

By substituting Eq. (11) into Eq. (3) integrated with z and substituting Eq. (3) into Eq. (2), oscillatory displacement fields can be obtained. Oscillatory displacement fields with odd power series ($n=1,3,5,\ldots$) for material 1 can be represented as

$$u_{xn}=\sum_{n=\text{odd}}^{\infty}\frac{K_n^0}{\sqrt{2\pi}(n^2+4\varepsilon^2)D\,\cosh\varepsilon\pi}\Bigg\{e^{\varepsilon(\pi-\theta_l)}p_l\overline{A}\Big[n\,\cos\Big(\varepsilon\,\ln r_l+\frac{n}{2}\theta_l\Big)+2\varepsilon\,\sin\Big(\varepsilon\,\ln r_l+\frac{n}{2}\theta_l\Big)\Big]r_l^{n/2}$$
$$+e^{-\varepsilon(\pi-\theta_l)}p_lA\Big[n\,\cos\Big(\varepsilon\,\ln r_l-\frac{n}{2}\theta_l\Big)+2\varepsilon\,\sin\Big(\varepsilon\,\ln r_l-\frac{n}{2}\theta_l\Big)\Big]r_l^{n/2}-e^{\varepsilon(\pi-\theta_s)}p_s\overline{B}\Big[n\,\cos\Big(\varepsilon\,\ln r_s+\frac{n}{2}\theta_s\Big)$$
$$+2\varepsilon\,\sin\Big(\varepsilon\,\ln r_s+\frac{n}{2}\theta_s\Big)\Big]r_s^{n/2}-e^{-\varepsilon(\pi-\theta_s)}p_sB\Big[n\,\cos\Big(\varepsilon\,\ln r_s-\frac{n}{2}\theta_s\Big)+2\varepsilon\,\sin\Big(\varepsilon\,\ln r_s-\frac{n}{2}\theta_s\Big)\Big]r_s^{n/2}\Bigg\}$$
$$+\sum_{n=\text{odd}}^{\infty}\frac{K_n^*}{\sqrt{2\pi}(n^2+4\varepsilon^2)D\,\cosh\varepsilon\pi}\Bigg\{-e^{\varepsilon(\pi-\theta_l)}p_l\overline{A}\Big[n\,\sin\Big(\varepsilon\,\ln r_l+\frac{n}{2}\theta_l\Big)-2\varepsilon\,\cos\Big(\varepsilon\,\ln r_l+\frac{n}{2}\theta_l\Big)\Big]r_l^{n/2}$$
$$-e^{-\varepsilon(\pi-\theta_l)}p_lA\Big[n\,\sin\Big(\varepsilon\,\ln r_l-\frac{n}{2}\theta_l\Big)-2\varepsilon\,\cos\Big(\varepsilon\,\ln r_l-\frac{n}{2}\theta_l\Big)\Big]r_l^{n/2}+e^{\varepsilon(\pi-\theta_s)}p_s\overline{B}\Big[n\,\sin\Big(\varepsilon\,\ln r_s+\frac{n}{2}\theta_s\Big)$$
$$-2\varepsilon\,\cos\Big(\varepsilon\,\ln r_s+\frac{n}{2}\theta_s\Big)\Big]r_s^{n/2}+e^{-\varepsilon(\pi-\theta_s)}p_sB\Big[n\,\sin\Big(\varepsilon\,\ln r_s-\frac{n}{2}\theta_s\Big)-2\varepsilon\,\cos\Big(\varepsilon\,\ln r_s-\frac{n}{2}\theta_s\Big)\Big]r_s^{n/2}\Bigg\} \tag{18}$$

$$u_{yn}=\sum_{n=\text{odd}}^{\infty}\frac{K_n^0}{\sqrt{2\pi}(n^2+4\varepsilon^2)D\cosh\varepsilon\pi}\Bigg\{e^{\varepsilon(\pi-\theta_l)}q_l\overline{A}\Big[n\sin\Big(\varepsilon\ln r_l+\frac{n}{2}\theta_l\Big)-2\varepsilon\cos\Big(\varepsilon\ln r_l+\frac{n}{2}\theta_l\Big)\Big]r_l^{n/2}$$
$$-e^{-\varepsilon(\pi-\theta_l)}q_lA\Big[n\sin\Big(\varepsilon\ln r_l-\frac{n}{2}\theta_l\Big)-2\varepsilon\cos\Big(\varepsilon\ln r_l-\frac{n}{2}\theta_l\Big)\Big]r_l^{n/2}-e^{\varepsilon(\pi-\theta_s)}q_s\overline{B}\Big[n\sin\Big(\varepsilon\ln r_s+\frac{n}{2}\theta_s\Big)$$
$$-2\varepsilon\cos\Big(\varepsilon\ln r_s+\frac{n}{2}\theta_s\Big)\Big]r_s^{n/2}+e^{-\varepsilon(\pi-\theta_s)}q_sB\Big[n\sin\Big(\varepsilon\ln r_s-\frac{n}{2}\theta_s\Big)-2\varepsilon\cos\Big(\varepsilon\ln r_s-\frac{n}{2}\theta_s\Big)\Big]r_s^{n/2}\Bigg\}$$
$$+\sum_{n=\text{odd}}^{\infty}\frac{K_n^*}{\sqrt{2\pi}(n^2+4\varepsilon^2)D\cosh\varepsilon\pi}\Bigg\{e^{\varepsilon(\pi-\theta_l)}q_l\overline{A}\Big[n\cos\Big(\varepsilon\ln r_l+\frac{n}{2}\theta_l\Big)+2\varepsilon\sin\Big(\varepsilon\ln r_l+\frac{n}{2}\theta_l\Big)\Big]r_l^{n/2}$$
$$-e^{-\varepsilon(\pi-\theta_l)}q_lA\Big[n\cos\Big(\varepsilon\ln r_l-\frac{n}{2}\theta_l\Big)+2\varepsilon\sin\Big(\varepsilon\ln r_l-\frac{n}{2}\theta_l\Big)\Big]r_l^{n/2}-e^{\varepsilon(\pi-\theta_s)}q_s\overline{B}\Big[n\cos\Big(\varepsilon\ln r_s+\frac{n}{2}\theta_s\Big)$$
$$+2\varepsilon\sin\Big(\varepsilon\ln r_s+\frac{n}{2}\theta_s\Big)\Big]r_s^{n/2}+e^{-\varepsilon(\pi-\theta_s)}q_sB\Big[n\cos\Big(\varepsilon\ln r_s-\frac{n}{2}\theta_s\Big)+2\varepsilon\sin\Big(\varepsilon\ln r_s-\frac{n}{2}\theta_s\Big)\Big]r_s^{n/2}\Bigg\}\tag{19}$$

where $n>0$. For material 2, which is the material below the interface, parameters $\varepsilon\pi$ and $-\varepsilon\pi$ in oscillatory stress and displacement fields are changed to $-\varepsilon\pi$, $\varepsilon\pi$. When n is 1, Eqs. (15)–(19) are stress and displacement fields around the propagating interfacial crack tip. Thus, K_1^0 and K_1^* are stress intensity factors K_{I} and K_{II}.

2.2 Nonoscillatory Stress and Displacement Fields. The λ_n is a positive integer eigenvalue in this case. Nonoscillatory stress fields with the even power series ($n=2,4,6,\ldots$) for material 1 can be presented as

$$\sigma_{xn}=\sum_{n=\text{even}}^{\infty}\frac{K_n^0}{\sqrt{2\pi}}\frac{1}{1+w_s}\frac{(1+M_a)}{D}\Bigg\{(M_b-q^2)r_s^{(n-2)/2}\times\cos\frac{n-2}{2}\theta_s-(M_b-p^2)r_l^{(n-2)/2}\cos\frac{n-2}{2}\theta_l\Bigg\}$$
$$+\sum_{n=\text{even}}^{\infty}\frac{K_n^*}{\sqrt{2\pi}}\frac{1}{1+w_l}\frac{1}{D}\Bigg\{\alpha_l(M_b-q^2)r_s^{(n-2)/2}\times\sin\frac{n-2}{2}\theta_s-\alpha_s(M_b-p^2)r_l^{(n-2)/2}\sin\frac{n-2}{2}\theta_l\Bigg\}\tag{20}$$

$$\sigma_{yn}=\sum_{n=\text{even}}^{\infty}\frac{K_n^0}{\sqrt{2\pi}}\frac{1}{1+w_s}\frac{(1+M_a)^2}{D}\Bigg\{r_s^{(n-2)/2}\cos\frac{n-2}{2}\theta_s-r_l^{(n-2)/2}\cos\frac{n-2}{2}\theta_l\Bigg\}+\sum_{n=\text{even}}^{\infty}\frac{K_n^*}{\sqrt{2\pi}}\frac{1}{1+w_l}\frac{(1+M_a)}{D}\times\Bigg\{\alpha_lr_s^{(n-2)/2}\sin\frac{n-2}{2}\theta_s-\alpha_sr_l^{(n-2)/2}\sin\frac{n-2}{2}\theta_l\Bigg\}\tag{21}$$

$$\tau_{xyn}=\sum_{n=\text{even}}^{\infty}\frac{K_n^0}{\sqrt{2\pi}}\frac{1}{1+w_s}\frac{(1+M_a)}{D}\Bigg\{\alpha_sr_s^{(n-2)/2}\sin\frac{n-2}{2}\theta_s-\alpha_lr_l^{(n-2)/2}\sin\frac{n-2}{2}\theta_l\Bigg\}+\sum_{n=\text{even}}^{\infty}\frac{K_n^*}{\sqrt{2\pi}}\frac{1}{1+w_l}\frac{\alpha_l\alpha_s}{D}\times\Bigg\{-r_s^{(n-2)/2}\cos\frac{n-2}{2}\theta_s+r_l^{(n-2)/2}\cos\frac{n-2}{2}\theta_l\Bigg\}\tag{22}$$

where $n>0$, $w_s=(l_{12})_1/(l_{12})_2$, and $w_l=(l_{21})_1/(l_{21})_2$.

Nonoscillatory displacement fields with even power series ($n=2,4,6,\ldots$) for material 1 can be represented as

$$u_{xn}=\sum_{n=\text{even}}^{\infty}\frac{K_n^0}{\sqrt{2\pi}}\frac{2}{1+w_s}\frac{(1+M_a)}{Dn}\Bigg\{p_sr_s^{n/2}\cos\frac{n}{2}\theta_s-p_lr_l^{n/2}\cos\frac{n}{2}\theta_l\Bigg\}+\sum_{n=\text{even}}^{\infty}\frac{K_n^*}{\sqrt{2\pi}}\frac{2}{1+w_l}\frac{1}{Dn}\Bigg\{\alpha_lp_sr_s^{n/2}\sin\frac{n}{2}\theta_s-\alpha_sp_lr_l^{n/2}\sin\frac{n}{2}\theta_l\Bigg\}\tag{23}$$

$$u_{yn}=\sum_{n=\text{even}}^{\infty}\frac{K_n^0}{\sqrt{2\pi}}\frac{2}{1+w_s}\frac{(1+M_a)}{Dn}\times\Bigg\{q_sr_s^{n/2}\sin\frac{n}{2}\theta_s-q_lr_l^{n/2}\sin\frac{n}{2}\theta_l\Bigg\}+\sum_{n=\text{even}}^{\infty}\frac{K_n^*}{\sqrt{2\pi}}\frac{2}{1+w_l}\frac{1}{Dn}\times\Bigg\{-\alpha_lq_sr_s^{n/2}\cos\frac{n}{2}\theta_s+\alpha_sq_lr_l^{n/2}\cos\frac{n}{2}\theta_l\Bigg\}.\tag{24}$$

For material 2, which is the material below the interface, parameters w_s and w_l are changed to w_s^{-1} and w_l^{-1}. Therefore, general stress and displacement fields for propagating the interface crack can be represented as

$$\sigma_n(r,\theta)=\sum_{n=1}^{\infty}[\sigma_{xn}\ \ \sigma_{yn}\ \ \tau_{xyn}]^T$$
$$u_n(r,\theta)=\sum_{n=1}^{\infty}[u_{xn}\ \ u_{yn}]^T.\tag{25}$$

2.3 Stress and Displacement Fields at the Interfacial Propagating Crack Tip. When n is 1, the general fields become the propagating crack-tip fields. Stress and displacement components σ_x, u_x at the interfacial propagating crack tip for material 1 are expressed as

$$\sigma_x=\frac{K_{\mathrm{I}}}{2\sqrt{2\pi}rD\,\cosh\,\varepsilon\pi}\left\{(M_b-p^2)f_l(\theta)\left[e^{\varepsilon(\pi-\theta_l)}\overline{A}\,\cos\left(\varepsilon\,\ln\,r_l-\frac{\theta_l}{2}\right)+e^{-\varepsilon(\pi-\theta_l)}A\,\cos\left(\varepsilon\,\ln\,r_l+\frac{\theta_l}{2}\right)\right]\right.$$
$$\left.-(M_b-q^2)f_s(\theta)\left[e^{\varepsilon(\pi-\theta_s)}\overline{B}\,\cos\left(\varepsilon\,\ln\,r_s-\frac{\theta_s}{2}\right)+e^{-\varepsilon(\pi-\theta_s)}B\,\cos\left(\varepsilon\,\ln\,r_s+\frac{\theta_s}{2}\right)\right]\right\}$$
$$+\frac{K_{\mathrm{II}}}{2\sqrt{2\pi}rD\,\cosh\,\varepsilon\pi}\left\{-(M_b-p^2)f_l(\theta)\left[e^{\varepsilon(\pi-\theta_l)}\overline{A}\,\sin\left(\varepsilon\,\ln\,r_l-\frac{\theta_l}{2}\right)+e^{-\varepsilon(\pi-\theta_l)}A\,\sin\left(\varepsilon\,\ln\,r_l+\frac{\theta_l}{2}\right)\right]\right.$$
$$\left.+(M_b-q^2)f_s(\theta)\left[e^{\varepsilon(\pi-\theta_s)}\overline{B}\,\sin\left(\varepsilon\,\ln\,r_s-\frac{\theta_s}{2}\right)+e^{-\varepsilon(\pi-\theta_s)}B\,\sin\left(\varepsilon\,\ln\,r_s+\frac{\theta_s}{2}\right)\right]\right\} \tag{26}$$

$$u_x=\frac{K_{\mathrm{I}}}{2D(1+4\varepsilon^2)\cosh\,\varepsilon\pi}\sqrt{\frac{2r}{\pi}}\left\{e^{\varepsilon(\pi-\theta_l)}p_l\overline{A}\left[\cos\left(\varepsilon\,\ln\,r_l+\frac{\theta_l}{2}\right)+2\varepsilon\,\sin\left(\varepsilon\,\ln\,r_l+\frac{\theta_l}{2}\right)\right]\frac{1}{f_l(\theta)}\right.$$
$$+e^{-\varepsilon(\pi-\theta_l)}p_lA\left[\cos\left(\varepsilon\,\ln\,r_l-\frac{\theta_l}{2}\right)+2\varepsilon\,\sin\left(\varepsilon\,\ln\,r_l-\frac{\theta_l}{2}\right)\right]\frac{1}{f_l(\theta)}-e^{\varepsilon(\pi-\theta_s)}p_s\overline{B}\left[\cos\left(\varepsilon\,\ln\,r_s+\frac{\theta_s}{2}\right)+2\varepsilon\,\sin\left(\varepsilon\,\ln\,r_s+\frac{\theta_s}{2}\right)\right]\frac{1}{f_s(\theta)}$$
$$\left.-e^{-\varepsilon(\pi-\theta_s)}p_sB\left[\cos\left(\varepsilon\,\ln\,r_s-\frac{\theta_s}{2}\right)+2\varepsilon\,\sin\left(\varepsilon\,\ln\,r_s-\frac{\theta_s}{2}\right)\right]\frac{1}{f_s(\theta)}\right\}$$
$$+\frac{K_{\mathrm{II}}}{2D(1+4\varepsilon^2)\cosh\,\varepsilon\pi}\sqrt{\frac{2r}{\pi}}\left\{-e^{\varepsilon(\pi-\theta_l)}p_l\overline{A}\left[\sin\left(\varepsilon\,\ln\,r_l+\frac{\theta_l}{2}\right)-2\varepsilon\,\cos\left(\varepsilon\,\ln\,r_l+\frac{\theta_l}{2}\right)\right]\frac{1}{f_l(\theta)}\right.$$
$$-e^{-\varepsilon(\pi-\theta_l)}p_lA\left[\sin\left(\varepsilon\,\ln\,r_l-\frac{\theta_l}{2}\right)-2\varepsilon\,\cos\left(\varepsilon\,\ln\,r_l-\frac{\theta_l}{2}\right)\right]\frac{1}{f_l}(\theta)+e^{\varepsilon(\pi-\theta_s)}p_s\overline{B}\left[\sin\left(\varepsilon\,\ln\,r_s+\frac{\theta_s}{2}\right)-2\varepsilon\,\cos\left(\varepsilon\,\ln\,r_s+\frac{\theta_s}{2}\right)\right]\frac{1}{f_s(\theta)}$$
$$\left.+e^{-\varepsilon(\pi-\theta_s)}p_sB\left[\sin\left(\varepsilon\,\ln\,r_s-\frac{\theta_s}{2}\right)-2\varepsilon\,\cos\left(\varepsilon\,\ln\,r_s-\frac{\theta_s}{2}\right)\right]\frac{1}{f_s(\theta)}\right\} \tag{27}$$

where

$$r_l=r\sqrt{\cos^2\theta+p^2\sin^2\theta},\quad r_s=r\sqrt{\cos^2\theta+q^2\sin^2\theta}$$
$$f_l(\theta)=[\cos^2\theta+p^2\sin^2\theta]^{-(1/4)},$$
$$f_s(\theta)=[\cos^2\theta+q^2\sin^2\theta]^{-(1/4)}$$
$$\theta_j=\tan^{-1}(Z_j\tan\theta),\quad j=l,s,\quad Z_l=p,\quad Z_s=q.$$

The displacements between the crack surfaces are given by

$$\delta(r)=\delta_2+i\,\eta\delta_1=\sqrt{\frac{2r}{\pi}}\,\frac{H_{21}(K_{\mathrm{I}}+iK_{\mathrm{II}})r^{i\varepsilon}}{(1+2i\varepsilon)\cosh(\varepsilon\pi)} \tag{28}$$

and the energy release rate is given by

$$G=\frac{(K_{\mathrm{I}}^2+K_{\mathrm{II}}^2)H_{21}}{4\,\cosh^2(\varepsilon\pi)}. \tag{29}$$

As the stress σ_x is taken to be discontinuous and strain ε_x to be continuous across the line $y=0$, the relation between $(\sigma_x)_1$ and $(\sigma_x)_2$ is the same as

$$(\sigma_x)_2=\frac{(a_{11})_1(\sigma_x)_1+[(a_{12})_1-(a_{12})_2]\sigma_y}{(a_{11})_2}. \tag{30}$$

From Eq. (13), the stress intensity factors for propagating the crack along the interface in the infinite plate are obtained as

$$K_{\mathrm{I}}+iK_{\mathrm{II}}=\sqrt{\pi a}(1+2i\varepsilon)(2a)^{-i\varepsilon}\left(\sigma_y^{\infty}+i\,\frac{1}{\eta}\,\tau_{xy}^{\infty}\right) \tag{31}$$

where σ_y^{∞} and τ_{xy}^{∞} are the applied normal and shear stresses at infinity. Since Eq. (31) contains the term $(2a)^{-i\varepsilon}$, the ambiguity of the dependence on the measuring unit of the crack length for the value of the stress intensity factor occurs. If $(r)^{-i\varepsilon}$ is replaced with $(r/l)^{-i\varepsilon}$ in Eq. (13), where $l=2a$ (crack length), the stress intensity factors become the following equation, which does not contain the ambiguity of the dependence on the measuring unit of the crack length:

$$K_{\mathrm{I}}+iK_{\mathrm{II}}=\sqrt{\pi a}(1+2i\varepsilon)\left(\sigma_y^{\infty}+i\,\frac{1}{\eta}\,\tau_{xy}^{\infty}\right). \tag{32}$$

When stress intensity factors are the same as in Eq. (32), the term $\varepsilon\,\ln\,r_k$ $(k=l,s)$ in Eqs. (15)–(19) and (26)–(27) is replaced by $\varepsilon\,\ln(r_k/2a)$.

3 Conclusions

General stress, displacement fields, and energy release rate are explicitly presented for the interfacial propagating crack in dissimilar orthotropic materials.

When the orthotropic materials have characteristic roots $m_l\approx i$ and $m_s\approx i$ in the stationary crack state, the fields are the same as the Deng [2] results for the propagating interfacial crack in isotropic bimaterials. When the mechanical properties of dissimilar orthotropic materials are the same, the stress, displacement fields, and energy release rate are the same as those of homogeneous orthotropic material [4]. When the interface crack propagation velocity is zero, the fields of the interfacial propagating crack are identical to those of the interfacial stationary crack. The results are useful for both dissimilar isotropic-isotropic and isotropic-orthotropic and orthotropic-orthotropic bimaterials under subsonic crack propagation velocity lower than the two Rayleigh wave velocities and homogeneous isotropic and orthotropic materials under subsonic crack propagation velocity.

Table 1 The comparison of dissimilar isotropic and orthotropic stress component $\sigma_x\sqrt{K_I}$ under plane stress ($c/C_{s1}=0.5$)

θ (deg)	Iso-Iso.Mat	Ort-Ort.Mat	θ (deg)	Iso-Iso.Mat	Ort-Ort.Mat
0^+	.634439	.6344413	0^-	1.503408	1.503400
10	.7468052	.7468115	−10	1.302192	1.302208
20	.8190195	.8190226	−20	1.064251	1.064264
30	.8481339	.8481356	−30	.8146014	.8146035
40	.8359575	.8359596	−40	.5795064	.5794959
50	.7908002	.7907966	−50	.382161	.3821618
60	.7287843	.7287816	−60	.2386282	.2386150
70	.6730161	.6730131	−70	.1543843	.1543860
80	.6487839	.6487848	−80	.1229814	.1229963
90	.6748663	.6748638	−90	.1271673	.1271672
100	.7547211	.7547229	−100	.1428393	.1428359
110	.8735087	.8735143	−110	.1447629	.1447555
120	1.00348	1.003481	−120	.1124064	.1124141
130	1.114235	1.114237	−130	.0342066	.0341946
140	1.181642	1.181642	−140	−.0908023	−.0908047
150	1.191849	1.191844	−150	−.2536999	−.2537051
160	1.14096	1.140951	−160	−.4382891	−.4383058
170	1.032682	1.032665	−170	−.6245366	−.6245342
180	.8758961	.8758781	−180	−.7919333	−.7919445

Appendix

- Properties of isotropic-isotropic bimaterial:

$$C_{s2}/C_{s1}=2,\ \ \nu_1=0.3,\ \ \nu_2=0.2,\ \ \rho_1=\rho_2,\ \ r=0.01.$$

- Properties of orthotropic-orthotropic bimaterial:

$$C_{s2}/C_{s1}=2,\ \ \nu_{LT1}=0.3,\ \ \nu_{LT2}=0.2,\ \ \rho_1=\rho_2,\ \ r=0.01$$

$$E_{L1}:E_{T1}:G_{LT1}=2.6000001:2.6:1,\ \ C_{sk}=(\sqrt{G_{LT}/\rho})_k$$

$$E_{L2}:E_{T2}:G_{LT2}=9.600001:9.6:4,\ \ \overline{K_I}=K_I/\sqrt{2\pi r}$$

$$\alpha_1=\alpha_2=90\ \text{deg}.$$

E_L, E_T, G_{LT}, and $\nu_{LT}(-\varepsilon_T/\varepsilon_L)$ are elastic constants and Poisson's ratio, L and T are, respectively, the fiber direction and the transverse direction to the fiber, while α is the angle of the fiber direction with respect to the crack direction. The above orthotropic materials are almost like the isotropic ones ($m_l\approx i$ and $m_s\approx i$ in $c/C_{s1}=0$). As shown in Table 1, when the orthotropic materials have isotropic characteristics, the fields derived in this study are the same as the Deng's ([2]) results of the interfacial propagating crack in isotropic bimaterials.

Acknowledgment

This research was supported by research funds from the Korea Science and Engineering Foundation under Grant No. 971-1003-017-2.

References

[1] Yang, W., Suo, Z., and Shih, C. F., 1991, ''Mechanics of Dynamic Debonding,'' Proc. R. Soc. London, Ser. A, **433**, pp. 679–697.
[2] Deng, X., 1993, ''General Crack-Tip Fields for Stationary and Steadily Growing Interface Cracks in Anisotropic Bimaterials,'' J. Appl. Mech., **60**, pp. 183–189.
[3] Liu, C., Lambros, J., and Rosakis, A. J., 1993, ''Highly Transient Elastodynamic Crack Growth in a Bimaterial Interface: Higher Order Asymptotic Analysis and Optical Experiments,'' J. Mech. Phys. Solids, **41**, No. 12, pp. 1887–1954.
[4] Lee, K. H., Hawong, J. S., and Choi, S. H., 1996, ''Dynamic Stress Intensity Factors K_I, K_{II}, and Dynamic Crack Propagation Characteristics of Orthotropic Material,'' Eng. Fract. Mech., **53**, No. 1, pp. 119–140.
[5] Lekhnitskii, S. G., 1963, *Theory of Elasticity of an Anisotropic Elastic Body*, Holden-Day, San Francisco.